Visibility Laboratory
University of California
Scripps Institution of Oceanography
San Diego 52, California

RESTORATION OF ATMOSPHERICALLY DISTORTED IMAGES

PROGRESS REPORT

by

James L. Harris

March 1963

SIO Ref. 63-10

Bureau of Ships
Contract NObs-84075, Assign. No. 2
Advanced Research Projects Agency
Order No. 152-60, Project No. 7400

Approved:

S. Q. Duntley, Director
Visibility Laboratory

TABLE OF CONTENTS

APPENDICES

LIST OF FIGURES

FIGURES IN APPENDIX III

RESTORATION OF ATMOSPHERICALLY DISTORTED IMAGES

PROGRESS REPORT

by

James L. Harris

1.0 STATEMENT OF THE PROBLEM

The space age has created renewed interest in the problems associated with optical observations from the ground of objects in space. It is possible to build large optical systems whose image quality is limited only by diffraction. In practice such ideal imagery is not obtained because of the image deterioration induced by atmospheric turbulence.

The Visibility Laboratory has been conducting a program of research on possible means of accomplishing restoration of these atmospherically distorted images. This work has been sponsored by the Advanced Research Projects Agency by transfer of funds to this Laboratory's existing Bureau of Ships contract NObs-84075. Considerable progress has been made in the development of techniques which may be suitable for the restoration of these images. This report summarizes the effort on this project from its conception in December of 1960 through December 1962.

The contents of this report have been placed in more or less historical order because the present day concepts have evolved from the earlier work and it is felt that the presentation in this

order of time may make it easier for the reader to follow the development.

2.0 SIMPLE MATHEMATICAL DISTORTIONS AND RESTORATIONS

2.1 Introduction

At the time that the project was initiated, specific image restoration techniques suitable for this application had yet to be developed. It was felt, however, that advances in technology in fields such as information theory, communication theory, and related sciences made it a reasonable time to take a new look at this very old problem.

Atmospheric turbulence can be said to be a form of noise acting on the image. Processes of extraction of signals in the presence of noise have long been used in radars and other sensors. Techniques of integrating many pulses in order to improve the signal-to-noise ratio have been utilized in radar systems since their development during World War II. This form of extraction of signal from noise, i.e., integration of signal and noise, is applicable in the radar case because the noise is additive. That is, the noise serves to amplitude modulate the signal. In the case of the image distortions due to atmospheric turbulence, the noise serves to smear the image spatially and it would therefore be expected that the direct integration techniques applicable to amplitude modulated noise conditions must be modified for this application.

2.2 An Example of a Simple Distortion and Restoration

A very early mathematical exercise of familiarization with spatial distortions may serve to demonstrate one way in which a series of distortions may be utilized to extract information by which a single image can be constructed whose image quality is superior to that of any of the individual distortions. Figure 1 shows a sample block letter and one possible distortion of the letter. The distortion is obtained by allowing each square forming the block to move left, right, up or down, each move with equal probability. In the case of this simple model, it was assumed that each square always moves, that is, the probability that a square will remain in its original position is zero. This simple model assumed that there were only two levels of intensity possible. If two elements from the original block letter moved into the same square, that square would become black and would not be distinguishable in level from a square which contained only one element from the original block letter. The manner in which the distorted image is formed may be observed by noting the arrows in Fig. 1 showing the movement of each of the original elements of the block letter. Figure 2 shows 17 distortions of an arbitrarily selected block letter. Based on observations of the 17 distortions, it is not apparent which block letter is actually present.

For this type of distortion, restoration can be accomplished by what has been termed "forbidden image diagrams." If, in the distortion, we can find a blank square which is bounded above, below, to the left and to the right by blank squares, then we can

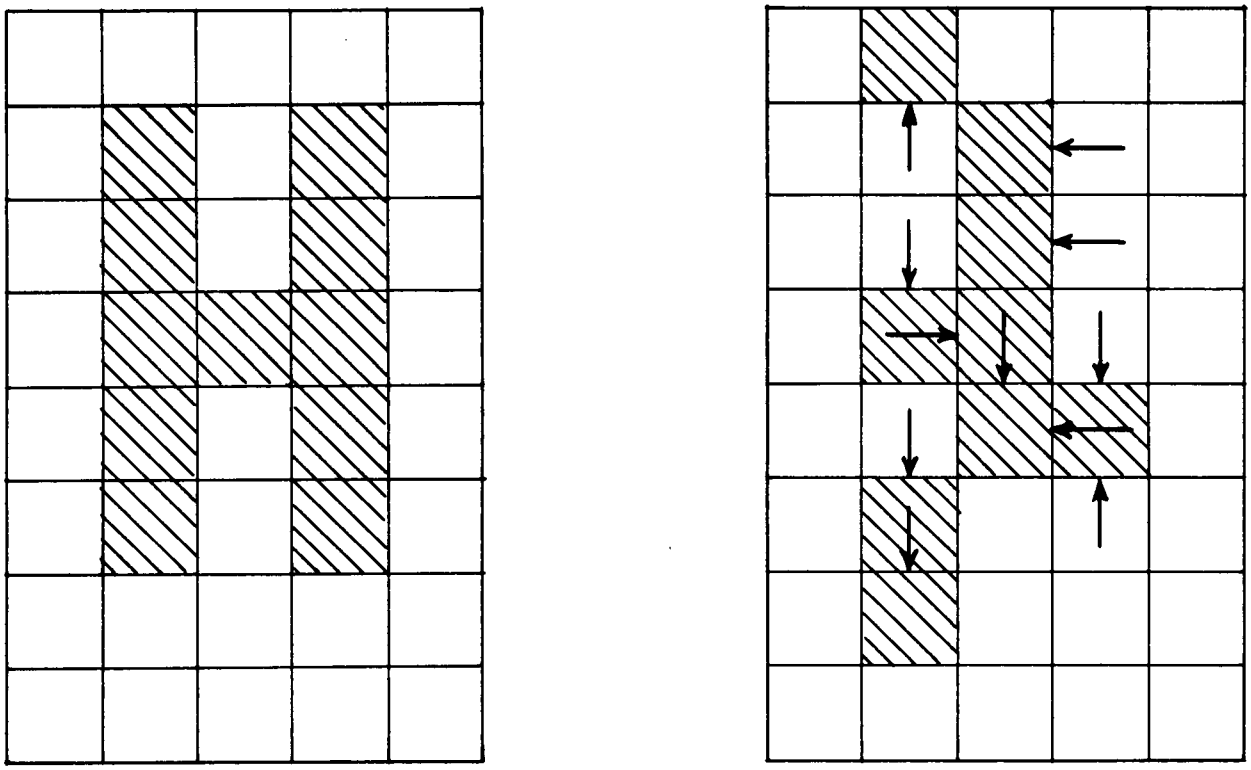

Figure 1. Sample block letter and a simple spatial distortion

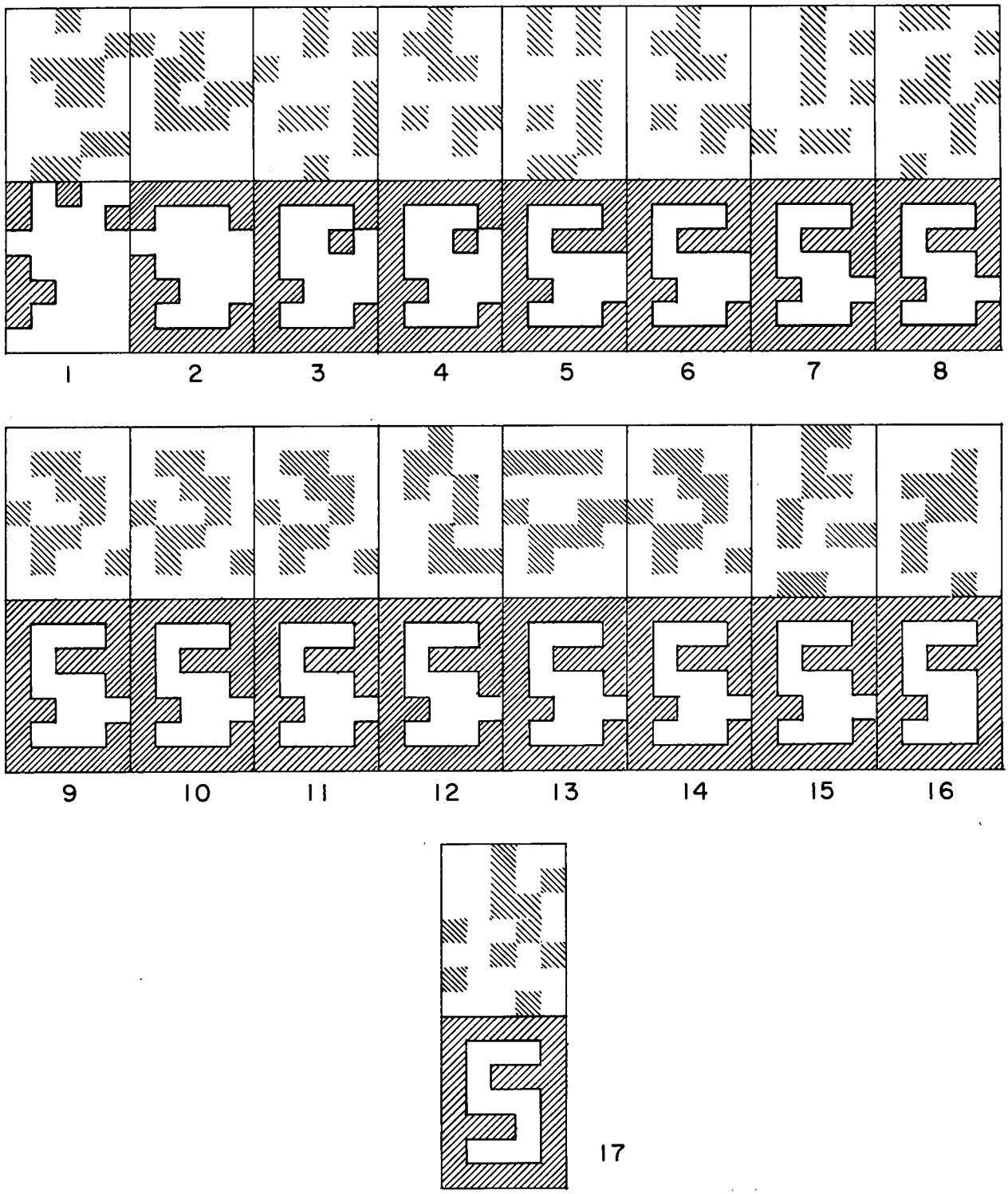

Figure 2. A simple spatial distortion and recovery

deduce that the original undistorted image was blank in the central square. This follows directly from the assumptions of the distortion since if the central square had contained an element, it is forced to move up, down, left or right, and hence would show up in the distortion in one of these squares. The "forbidden image diagram" for a single distortion is therefore a map which shows those increments which could not have contained an element of the target.

A "forbidden image diagram" can be made for each of the 17 distortions. Restorations are accomplished by noting that the "forbidden image diagrams" are cumulative; that is, we can superimpose each of the "forbidden image diagrams" to obtain the sum total of our information about those squares which could not have contained a target increment. Figure 2 also shows the construction of a cumulative "forbidden image diagram." The "forbidden image diagram" shown below distortion 2 contains those squares for which a target element could not be present as deduced from both distortion 1 and distortion 2. The "forbidden image diagram" below distortion 17 therefore contains all squares which are known to have not contained a target element as deduced from all 17 distortions. As may be seen from the figure, the block letter S, which was the block letter used in the distortions, has been successfully recovered.

The example which has been described was educational in that it demonstrated that, at least for this simple type distortion, there were techniques by which spatial distortions could utilize information from a large number of distortions to create a single image of quality superior to that of any of the individual distortions. The model, however, is not a realistic one in terms of the type of distortion to be found as the result of atmospheric turbulence.

3.0 INTRODUCTION TO SPATIAL FREQUENCIES

The later techniques of restoration employ the concepts of spatial frequencies and an introduction to these concepts will be made at this time.

Any function having only a finite number of discontinuities can be expressed over a defined region by an infinite series of sine and cosine terms. Thus the Fourier expansion of f(x) over an interval X is

$$f(x) = \frac{A_o}{2} + A_1\cos 2\pi fx + A_2\cos 4\pi fx + A_3\cos 6\pi fx + \ldots$$

$$+ B_1\sin 2\pi fx + B_2\sin 4\pi fx + B_3\sin 6\pi fx + \ldots \qquad (1)$$

where A_1, A_2, ..., B_1, B_2, ... are the sine and cosine coefficients which are defined by Eqs. (2) and (3).

$$A_i = \frac{2}{X}\int_{-\frac{X}{2}}^{+\frac{X}{2}} f(x)\cos(i2\pi fx)\,dx \qquad (2)$$

$$B_i = \frac{2}{X}\int_{-\frac{X}{2}}^{+\frac{X}{2}} f(x)\sin(i2\pi fx)\,dx \qquad (3)$$

This type of analysis has become widely known through its application to the analysis of electrical circuit problems, where a signal is described in terms of its frequency

composition. The importance of these concepts has been amply demonstrated in the case of radar, communications systems, and audio-amplifier design. In practical problems an infinite series is seldom involved and it is generally recognized that an approximation to a function can be made by including a finite number of terms with the degree of approximation dependent upon the number of such terms which are employed. There are obviously no restrictions on the dimensions of the function which is to be expanded in Fourier series. For example, the function might be voltage as a function of time, average annual rainfall as a function of latitude, or, as in the case of interest here, image intensity as a function of a spatial dimension.

Consider the case of a piece of film on which an image is stored. A complete description of the image involves the defining of the transmission of the film as a function of the X-Y coordinates of the film. If X is a horizontal dimension then it can be imagined that a trace in the X direction for a fixed Y will result in a function of transmission as a function of X. Since it is necessary to represent the image only over the film format, this transmission as a function of X can be expanded in a Fourier series. The coefficients for this expansion will be dependent upon the value of Y which was selected for the trace, that is, each of the coefficients is a function of Y. The coefficient itself can therefore be expanded in a Fourier series as a function of Y. If this is accomplished, as has been done in Appendix I, the result is a two-dimensional Fourier

series which describes the transmission of the film as a function of X and Y in terms of an infinite series of sine and cosine terms. One form of this two-dimensional Fourier series is

$$f(x,y) = A_o + \sum_{i=0}^{\infty} \sum_{j=0}^{\infty} A_{ij}\cos(2\pi i f_x x + 2\pi j f_y y)$$

$$+ \sum_{i=0}^{\infty} \sum_{j=0}^{\infty} B_{ij}\sin(2\pi i f_x x + 2\pi j f_y y) \qquad (4)$$

Each of the terms in this series expansion is a spatial sinusoid. Figure 3 is a sketch of one such sinusoidal component. The terms i and j indicate the number of cycles which the sine wave makes in the X and Y directions respectively; thus in the example shown, i = 3 and j = 4. One reason that the use of Fourier expansion has particular significance in optical systems is that an optical system passes no spatial frequencies above a defined cutoff frequency. A finite series is therefore all that is required to completely define a bounded optical image. It is shown in Appendix II that the statement of a cutoff frequency for the optical system is the Fourier equivalent of the usual statement with reference to the angular resolution associated with a diffraction limited optical system. Because of this spatial frequency cutoff in any real optical system, it is possible to define any real image by a finite set of numbers. The significance of this fact may be better appreciated after the development of those restoration techniques which employ the concepts of spatial frequencies.

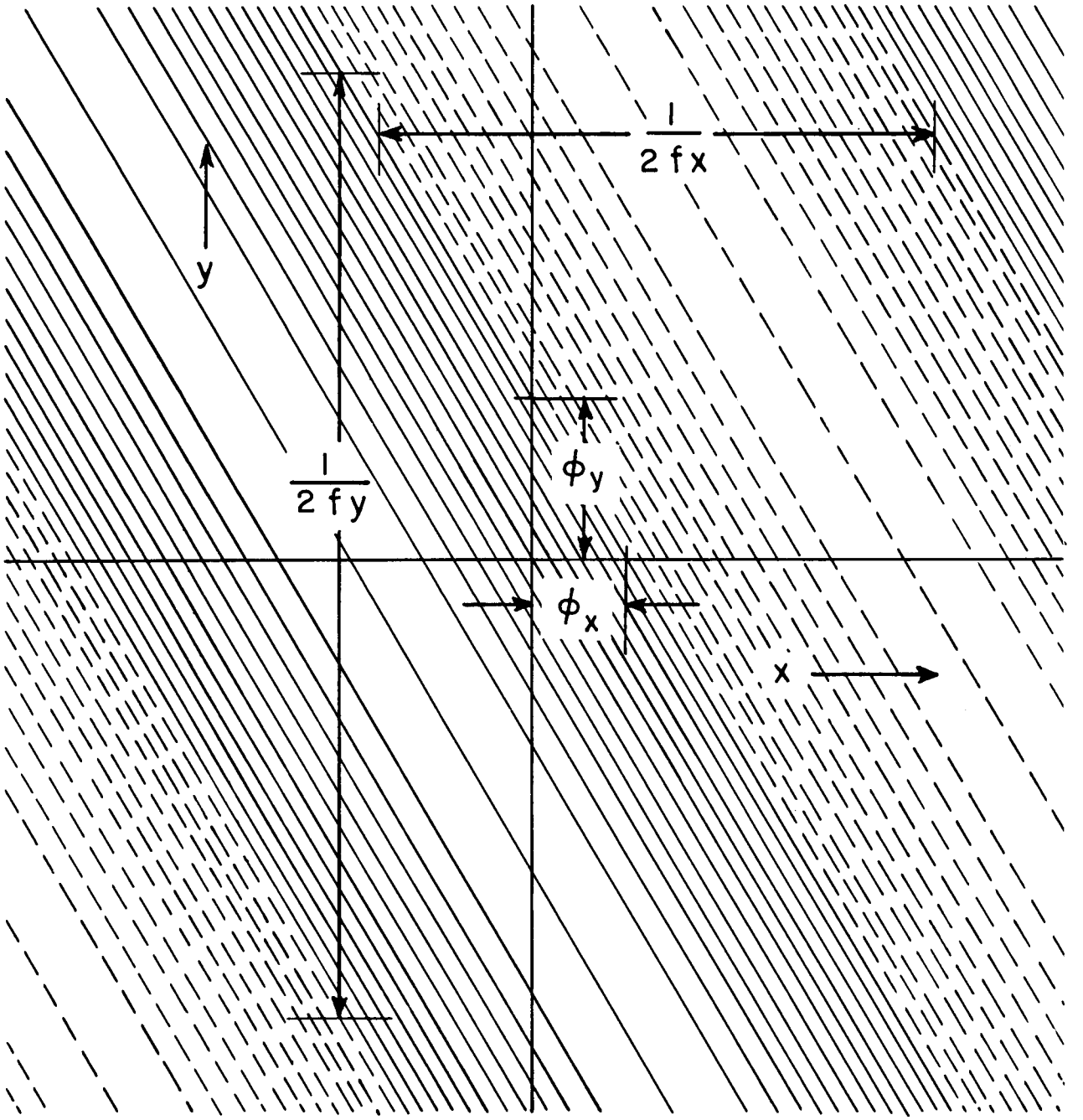

Figure 3 A Typical Spatial Frequency

4.0 A GEOMETRIC DISTORTION MODEL

4.1 Description of the Model

If a distant star is observed with an optical system having a small entrance pupil diameter, the primary effect of the atmospheric turbulence is to move the image about in a random fashion. This can be explained on the basis of the turbulence creating index of refraction gradients before the entrance pupil of the optical system, thus acting in the manner of a prism. These simple observations serve as a basis for a geometric model of image distortion due to atmospheric turbulence. In this model it is assumed that the entrance pupil can be quantized into sectors, each sector having a refractive index gradient which is determined in some statistical fashion. Figure 4 shows a cross section through an optical system, showing the manner in which the different sectors of the lens form images of the object displaced with respect to one another. The addition of these independent images is the resultant distorted image as predicted by this geometric model.

In order to more fully understand the nature of the distortion process, a single spatial frequency will be distorted in the same manner as indicated in Fig. 4. Figure 5 shows the separate images formed by each sector of the entrance pupil of the optical system and again schematically shows that each sector forms an image of the particular spatial frequency with the index of refraction gradient causing the image from each sector to be displaced right or left from the correct image

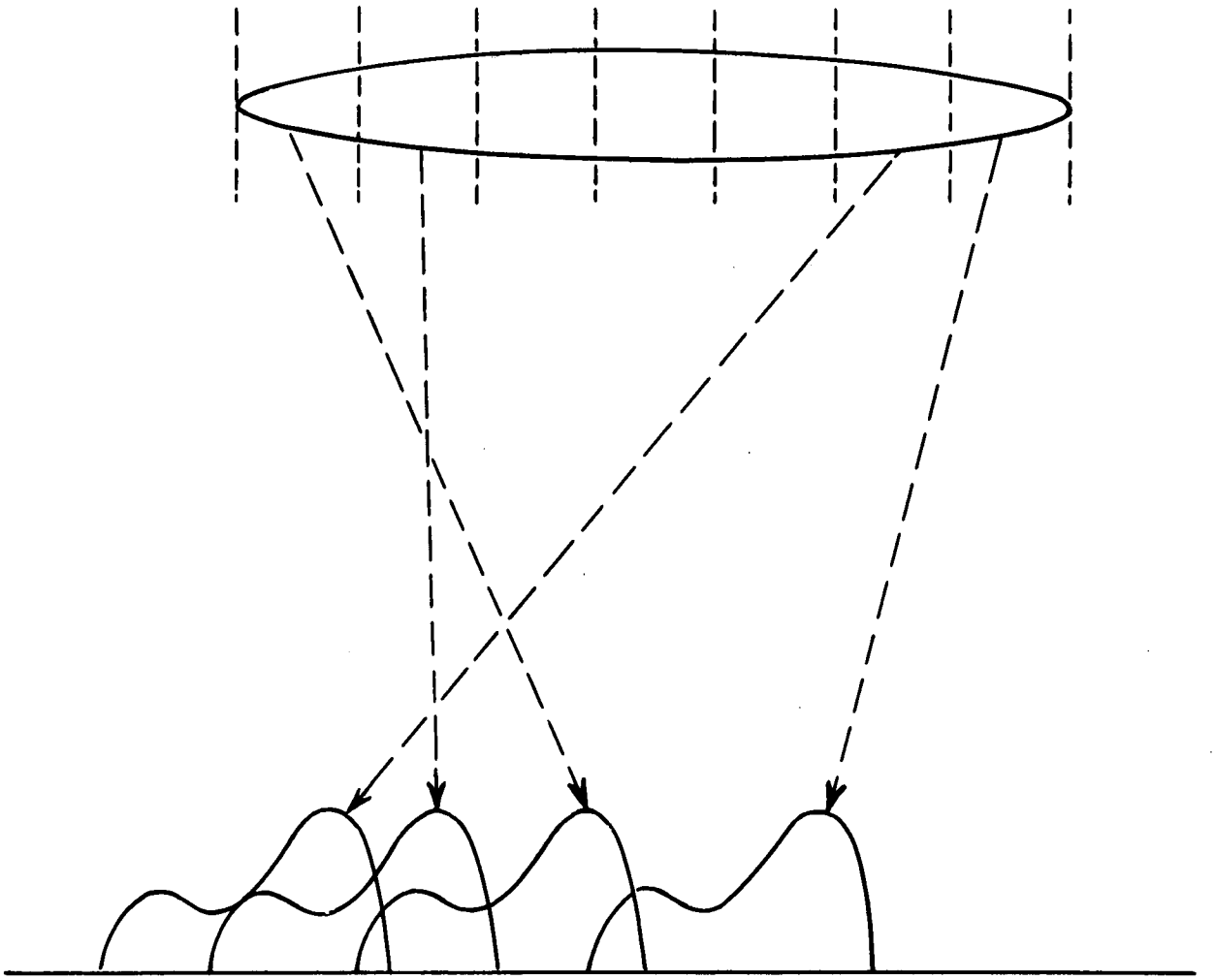

Figure 4 Schematic illustration of the nature of the geometric distortion.

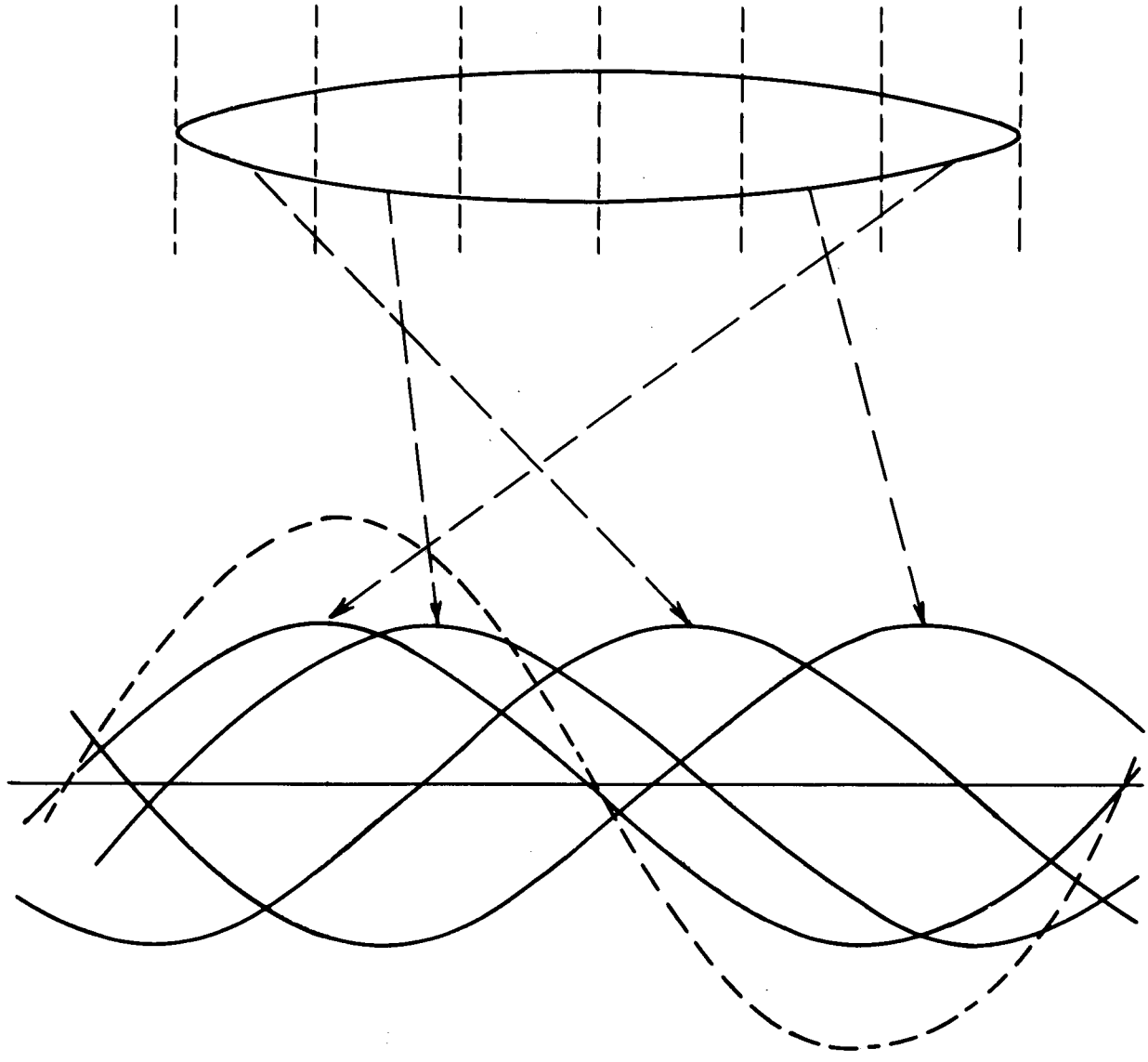

Figure 5 Geometric distortion of a single spatial frequency.

position. The composite image is, as before, the sum of the images from each section and in the case of the addition of the sinusoidal components, the resultant is also a sinusoid whose amplitude will always be less than the amplitude of an undistorted image, that is, the addition of sinusoids of different phases results in a sinusoid having an amplitude less than would be obtained had the phases been equal and having a phase shift with respect to the phase of the undistorted image. Thus, the geometric model predicts that in terms of spatial frequencies the effect of atmospheric turbulence is to attenuate the amplitude of the spatial frequency and shift its phase.

4.2 An Example of a Geometric Distortion

The distortion model described in the preceding paragraph was used to study possible restoration techniques. A necessary first step in the application of the model is the assumption of a probability distribution for displacement. As a matter of mathematical convenience, the displacement distribution or gradient distribution was chosen to be a triangular distribution as shown in Fig. 6. Since the distribution has symmetry about zero gradient, the average displacement is zero.

Figure 7 shows the undistorted image used in the example. Mathematically the image is a pulse as represented by the first ten Fourier coefficients. By analogy, it might be imagined that Fig. 7 represents a horizontal trace through the image of

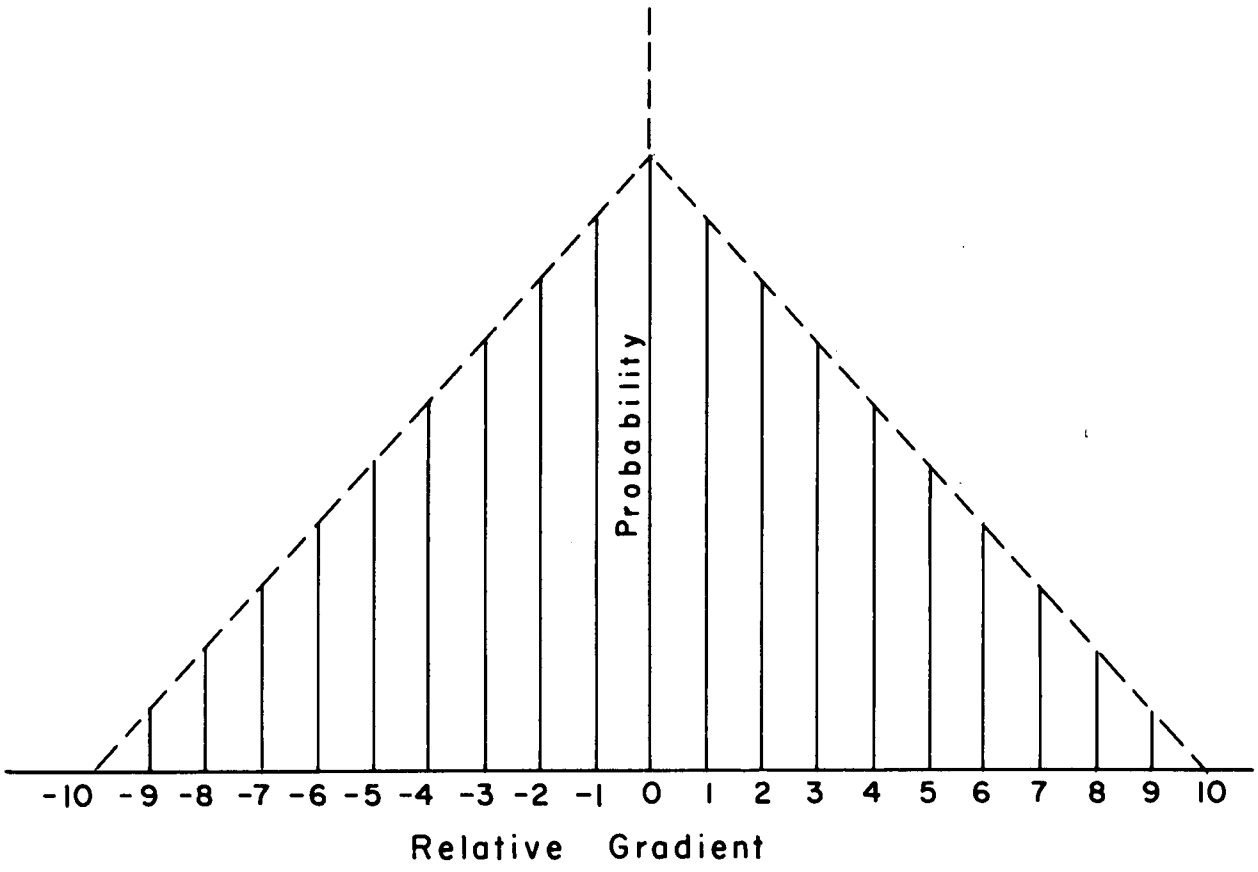

Figure 6 Probability distribution of the refractive gradient.

IMAGES AND THEIR SPECTRA

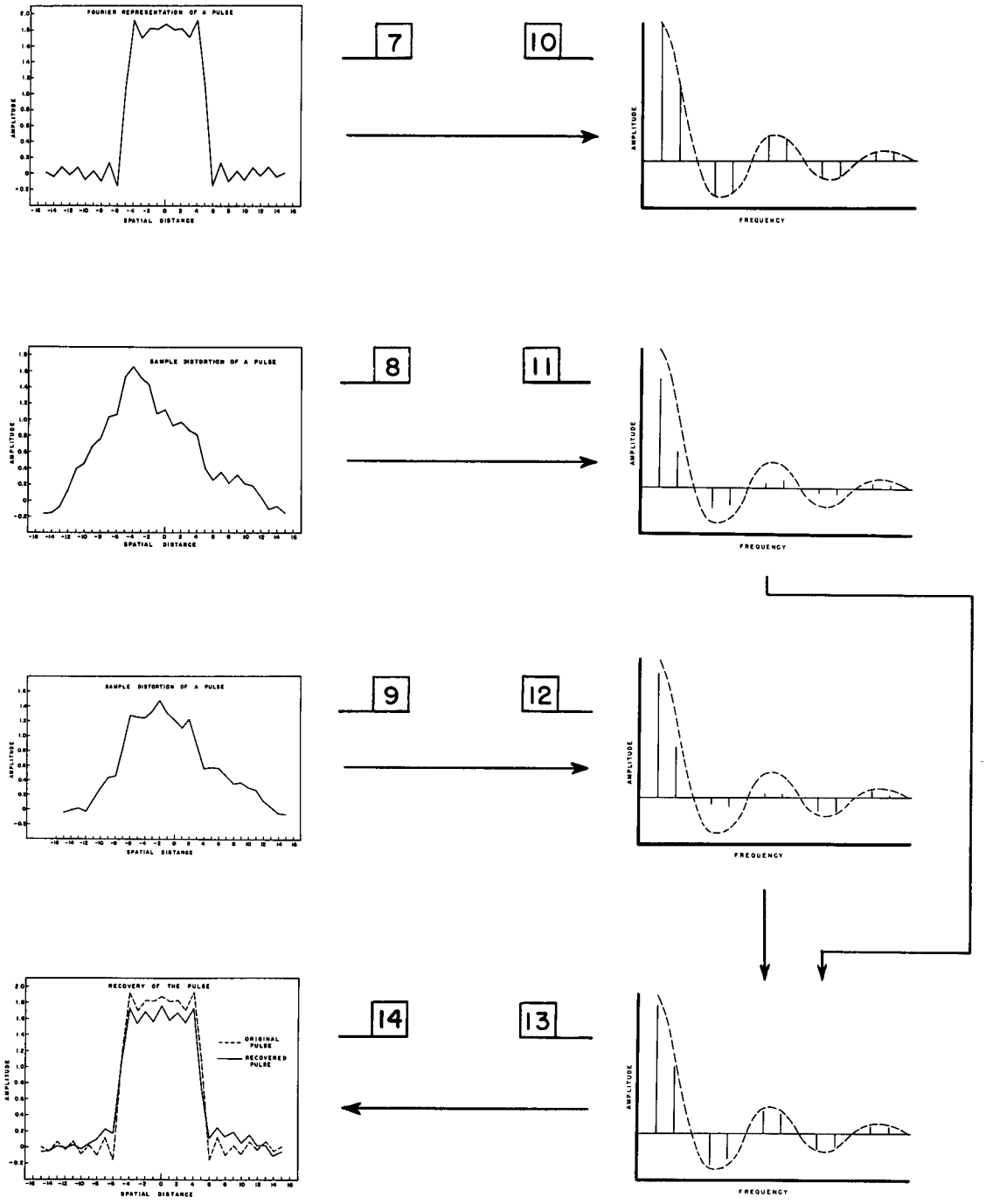

Figures 7 through 14

a vertical bar. The representation by a limited number of Fourier coefficients is a rough analogy to the diffraction limit because, as stated in Section 3.0, a diffraction limited optical system passes no frequencies above a definable cutoff value.

The image of Fig. 7 was subjected to the distortion process illustrated in Fig. 4 using the gradient distribution of Fig. 6. The lens was assumed to be divided into ten segments and by obtaining ten samples from the gradient distribution, sample distortions were constructed. Figures 8 and 9 are examples selected from a group of 30 such distortions.

It was noted in Section 4.1 that the effect of this geometric distortion is to attenuate and shift the phase of any given spatial frequency. This observation leads to one possible restoration technique which will now be illustrated. Figure 10 shows the spectrum of the undistorted image. The dashed line is the envelope and the vertical lines are the discrete frequencies of the Fourier series which represent the function over the extent of the image. Figures 11 and 12 show the spectra of the two sample distortions and indicate that the amplitude of any given spatial frequency varies from distortion to distortion. Since it has been observed that a spatial frequency is always attenuated in the process of distortion, a safe estimate is that the spatial frequencies in the undistorted image must have amplitudes at least as large as the highest amplitude found in any of the individual distortions. It may also be observed from studying the spectra of the three distortions that one distortion may produce a relatively unattenuated amplitude for one spatial

frequency whereas another spatial frequency in that same distortion may be quite heavily attenuated. It might therefore be expected that by selection of the highest amplitudes for all spatial frequencies from all distortions, information could be obtained which would be superior to the information which can be obtained from any one distortion. This process of sorting through a number of distortions and selecting the highest amplitudes for each spatial frequency has been termed the peak spectrum selection technique.

Thirty distortions of the type shown in Figs. 8 and 9 were constructed and their spectra generated. The spectra were then processed by the peak spectrum selection technique. Figure 13 shows the resultant spectrum obtained by selecting the peaks or maximum amplitudes from each of the thirty distortions. It may be noted that the spectrum thus obtained is a very close match to the undistorted spectrum, the envelope of which is shown as a dashed line. Phase information must also be processed. Since a symmetric type distortion process was assumed, that is, the image is equally likely shifted left or right, the average phase shift is 0, that is, it is equally probable that the phase shift will be positive or negative. A simple process of phase averaging, therefore, can be used to estimate the correct phase to be associated with each of the peak amplitudes. The recovered amplitude and phase information may now be utilized to construct a restoration of the distorted image. Figure 14 compares the image restoration generated in this matter with the original undistorted image shown with the dashed lines. While the recovery obtained was not

complete, the recovered image does bear close resemblance to the undistorted image and is far superior to any one of the thirty individual distortions utilized in the process. This latter point is significant since it indicates that this process involved something more than simply looking through a large series of distortions and selecting the best of these distorted images. This would be expected from the fact that the information which constitutes the recovered image was obtained not from a single distortion but from many of the thirty distortions.

5.0 COMPUTER PROGRAMING

The example of Section 4.0 clearly indicated the value of two-dimensional Fourier analysis as a tool in the processing of distorted images. These calculations were carried out on a desk calculator and required a great deal of time and effort in obtaining the recovered image of Fig. 14. It was recognized that if this technique was to have application to two-dimensional images having a large number of picture elements and for a large number of distortions, the hand calculator techniques must be replaced by computer operations.

The Computer Center of the School of Science and Engineering, University of California, San Diego, includes a Control Data Corporation 1604 computer with a 160-A satellite computer. Peripheral equipment includes an IBM-088 card reader, an Analex high speed printer, and necessary magnetic tape units. Computer programs for this project have been written in Fortran 60. The basic computer program consists of taking a series of input data

points which describe the image at points on an XY grid and performing two-dimensional Fourier analysis to obtain the amplitude and phase of each spatial frequency comprising the image. Additional subroutines allow for operation on these spatial frequencies in any desired fashion. For example one such subroutine allows the application of the peak selection technique and the phase averaging as utilized in Section 4.0. The computer output consists of tabulations of the amplitude and phase of each of the spatial frequencies for each image which has been inserted, as well as the peak amplitude and average phases associated with restorations achieved by the peak selection technique, and the restored image obtained by taking the inverse transformation of this peak selection phase averaged spectrum. Several auxiliary subroutines for displaying the output and input information have been developed and can be used as desired. As an example, the computer can take the output image, round each picture element to the nearest digit between one and ten, and print out an image having the proper XY relationship with this ten step gray scale.

An "image" printout was developed as an aid to immediate visual evaluation of the results. Printed patches of each character available in the Analex printer were photometered. The values obtained reflect the difference in inked areas associated with the different characters. The maximum reflectance is, of course, a blank and the minimum reflectance was found to be the character E. Characters of intermediate

reflectance were chosen to fill out a ten step gray scale as follows:

Character	Relative Reflectance
Blank	1.0
.	0.95
———	0.92
+	0.91
I	0.87
=	0.84
4	0.81
H	0.78
$	0.75
E	0.72

While the resulting printed images are lacking in contrast, they do allow a measure of visual evaluation. An example is shown in Fig. 15.

6.0 MATHEMATICAL MODEL OF ASTRONOMICAL DISTORTIONS

The example of Section 4.0, A Geometric Distortion Model, was extremely valuable as a means of investigating the application of Fourier techniques to restoration processes. It does not, however, represent an accurate model of the distortion process which would be expected by a large aperture optical system. The geometric distortion model assumed an intensity addition of images formed by the various sectors of the entrance pupil. This model, therefore, neglects the effect of the coherence of the wave front over the entire entrance pupil. While it is perfectly plausible to consider

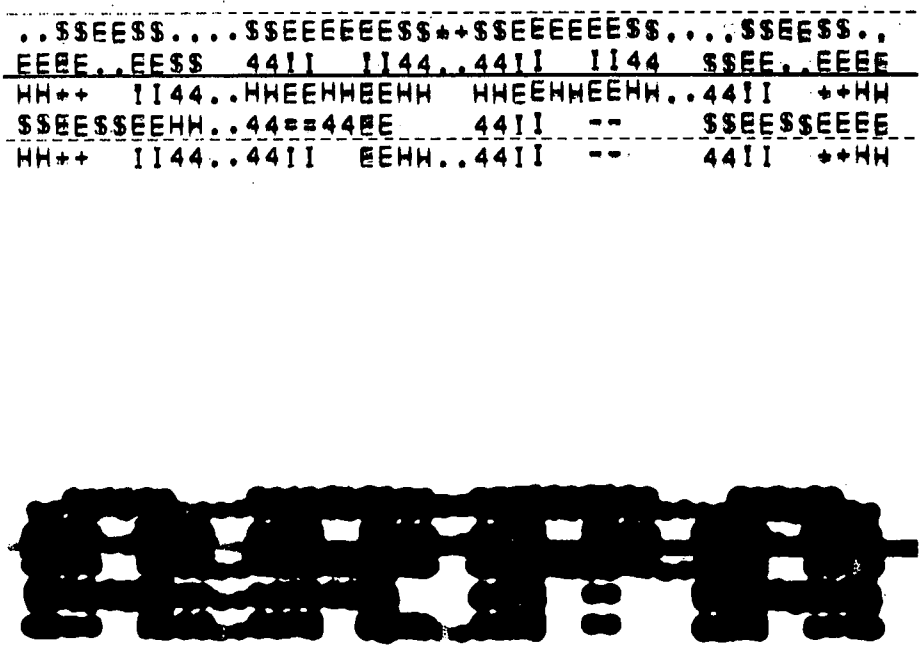

Figure 15 Direct Analex printer image readout.

separately the images formed by various sectors of the entrance pupil, these images will not be additive in intensity because of the coherence of the electromagnetic radiation. A more realistic model must consider the addition of these images with due consideration to the relative phase of the electromagnetic radiation as received from the different sectors. It will be shown that this distinction is an important one.

In Appendix II, it is shown that any two points on the entrance pupil serve to generate a single spatial frequency which has a sinusoidal variation in a direction parallel to the vector connecting the two points. For example, if the two points on the entrance pupil were chosen to fall on the X axis, the resultant image would be described by the equation

$$F(x) = A_1A_2 + A_1A_2 \sin\left(\frac{2\pi Dx}{\lambda f} + \Delta\phi\right) \qquad (5)$$

as illustrated in Fig. 16. The terms A_1 and A_2 are the amplitudes of the electromagnetic wave front at the two points on the entrance pupil, D is the distance between the two points on the entrance pupil, λ is the wave length of the radiation, f is the focal length of the optical system, x is the spatial dimension in the image plane, and $\Delta\phi$ is the phase difference between the electromagnetic radiation at the two points on the entrance pupil. For the case of atmospheric turbulence close to the entrance pupil, A_1 and A_2 would have approximately the same amplitude as in the absence of turbulence, and the primary image distortion

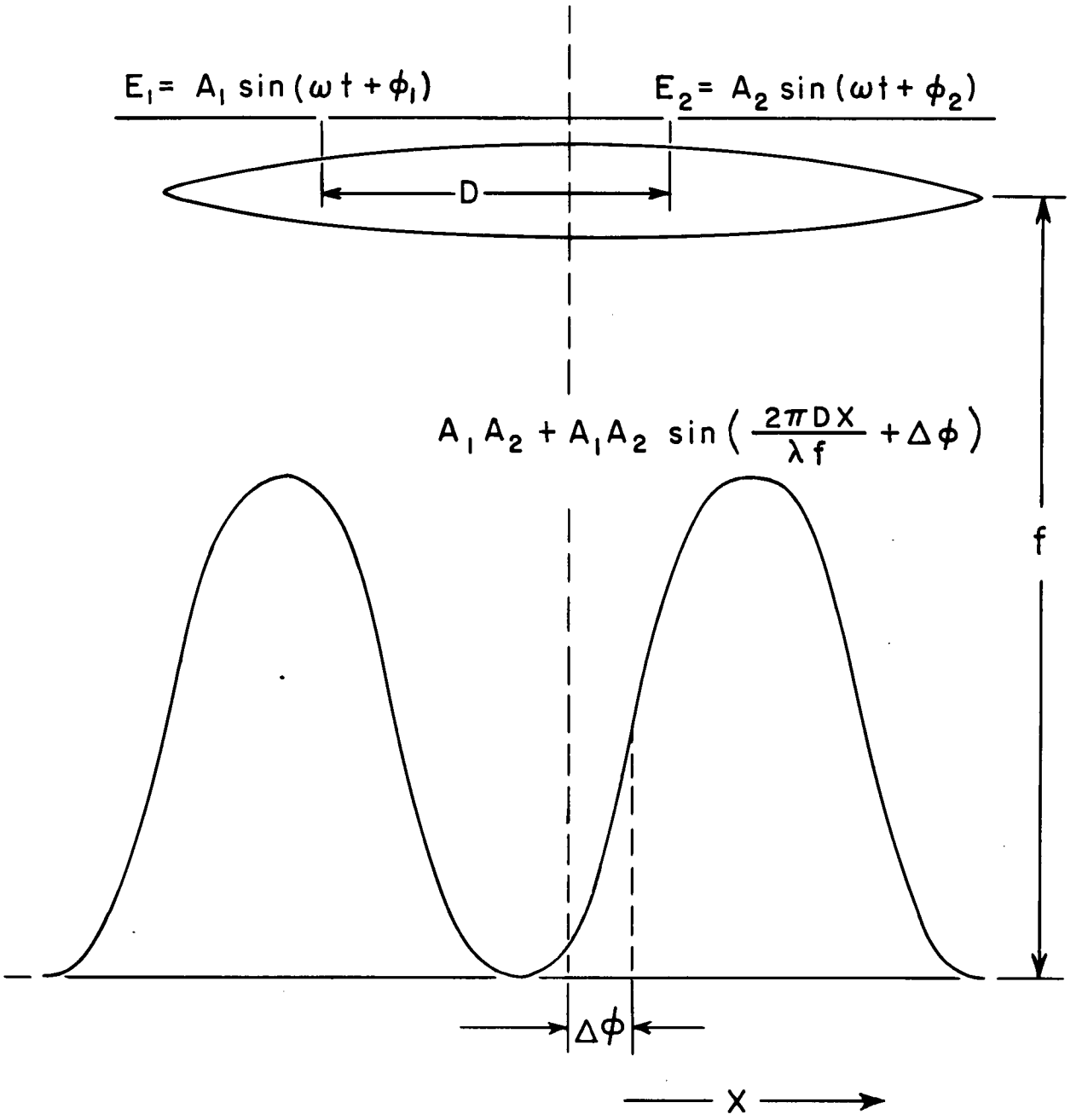

Figure 16 Intensity distribution from two points on the entrance pupil.

would be due to the $\Delta\phi$ term. Appendix II goes on to show that the total contribution to a given spatial frequency may be found by summing all of the sine terms of the type shown in Eq. (5) from every pair of points on the entrance pupil, separated vectorially by the distance D(see Eqs. II-15 and II-16). Figure 17 illustrates this point by showing that area of the entrance pupil which is responsible for the generation of a spatial frequency $\frac{D}{\lambda}$. This has been termed a spatial frequency zone.

As in the case of the geometric distortion, a maximum amplitude is obtained when all of the $\Delta\phi$'s are equal or equal to 0. This is the case of an undistorted image where the electromagnetic wave front is still plane at the time it reaches the entrance pupil. Thus it is once again apparent that the effect of atmospheric turbulence will be to attenuate the amplitude of any given spatial frequency. The peak spectrum selection technique utilized in restoration of the image distortions in Section 4.0 is therefore applicable to this more refined model of distortions due to atmospheric turbulence.

The distortion process may be visualized with reference to Fig. 16 by imagining a phase distortion map superimposed over the entrance pupil of the optical system. The amplitude of any spatial frequency in the resulting distorted image is found by summing all of the sine waves of Eq. (5) for every pair of points separated by a distance D as defined by the

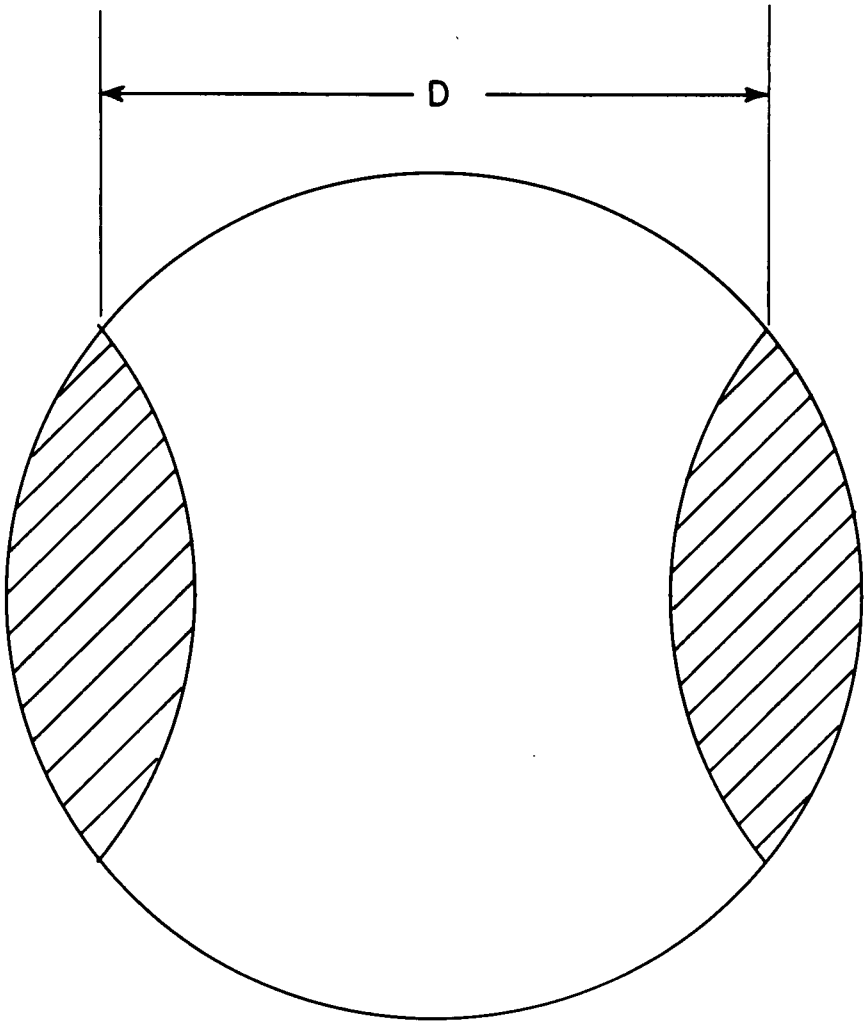

Figure 17 Entrance pupil zones making contribution to a spatial frequency $f = \frac{D}{\lambda}$.

zones of Fig. 17. A power spectrum may be associated with the phase distortion map.[1] This power spectrum will fall off as frequency is increased. The significance of this fact is that there will be no discontinuities or very rapid changes in the phase map over short distances. Two points on the phase map separated by a short distance will, therefore, be highly correlated. Since the very low frequencies passed by the optical system correspond to pairs of points separated by very short distance, there will be a tendency for the very low frequencies to be passed with small attenuation. For the higher frequencies which relate to points separated by increased distance, there will be an increased probability of having phase difference between the two points and, therefore, it is to be expected that as the frequency increases, the attenuation will increase. The increase in attenuation with frequency will continue until a frequency is reached at which the separation between the pairs of points which form this spatial frequency is sufficiently large, such that the phase variation at the two points becomes independent. From this point on there will be no increase in attenuation with frequency.

There is a very great significance to the assertion of the previous paragraph. Previous geometric models of the distortion process have suggested that the image of a point source in the presence of turbulence would be normally distributed in two dimensions. The Fourier transformation of a two-dimensional normal distribution is also a two-dimensional normal distribution.

[1] S. H. Reiger, "Seeing through the atmosphere," Proceedings of a Symposium, December 1962, Rand Corporation Memorandum RM-3294-PR.

Such a model suggests that there is an increase of attenuation with frequency without limit. This type of model would, therefore, impose a practical limit to the highest frequencies which could ever hope to be recovered or restored. The fact that the more realistic model indicates a leveling off of attenuation with the higher frequencies suggests that no such limit does, in fact, exist.

In addition to offering an explanation of the distortion process in the presence of atmospheric turbulence, the derivations of Appendix II also offer a ready means of determining the transfer function of a diffraction limited optical system. Since the contribution to a given spatial frequency can be associated with zones on the entrance pupil bounding all points separated by distance $D = f\lambda$, as illustrated in Fig. 17, the defining of these zones and the measurement of this area relative to the total area of the entrance pupil is, directly, the transmittance of the optical system for this given spatial frequency. This concept of zones associated with non-coherent optical systems is suggestive that where primary concern is for objects of high spatial frequency, techniques of apodization, that is, masking of the entrance pupil, may be effective in increasing the amplitude of the spatial frequencies relative to the average ambient amplitude.

7.0 REAL TURBULENCE DISTORTIONS AND RESTORATIONS

The peak spectrum selection technique introduced in Section 4.0 has also been utilized in attempts to restore images distorted by real turbulence. A six-inch diameter astronomical objective was mounted so as to form an image in the plane of a mechanically driven aperture. The flux passing through the aperture was collected on the photocathode of a multiplier phototube whose output was displayed on an oscilloscope. The scanning aperture performed a single horizontal scan and the resulting oscilloscope waveform was photographically recorded. The scanning apparatus was equipment available at the Laboratory as a result of work on a prior photoelectric scanning problem. A hot plate was mounted in front of and below the objective lens to produce turbulence close to the entrance pupil. The single horizontal scan was sufficiently fast so that the image was essentially fixed during the entire scan. In order to obtain high flux levels and therefore minimize the noise level relative to the signal level, the object to be imaged was chosen to be a filament lamp. Since the scan was performed in one dimension only, it was necessary that the image have flux variation in only one dimension. The image of the filament lamp satisfied this requirement in that for a considerable region in the image plane, it had the general appearance of being three vertical bars. Figure 18 shows thirty oscilloscope photographs, each representing one horizontal trace through the image of the filament lamp. The fourth recording in this series was taken with the hot plate removed in order to show

TURBULENCE-DISTORTED IMAGES & RESTORATIONS

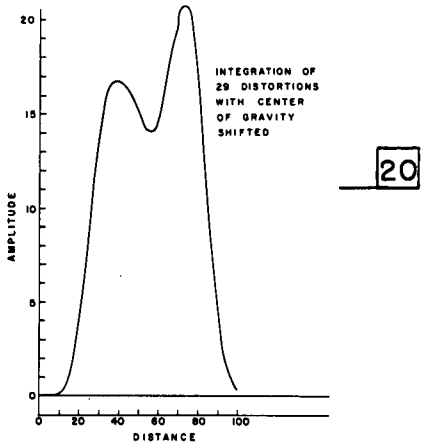

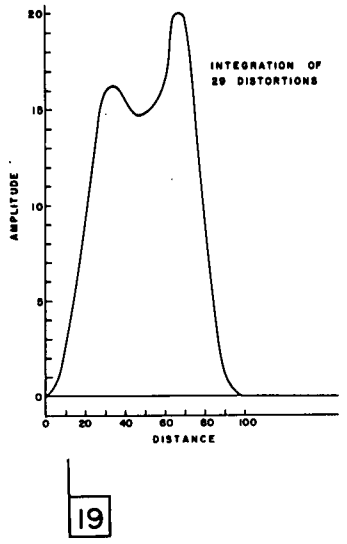

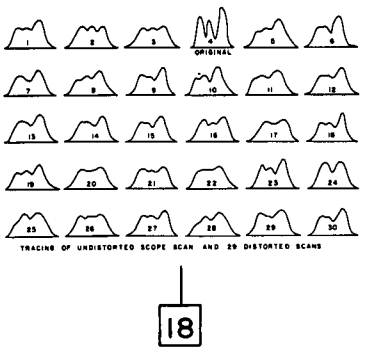

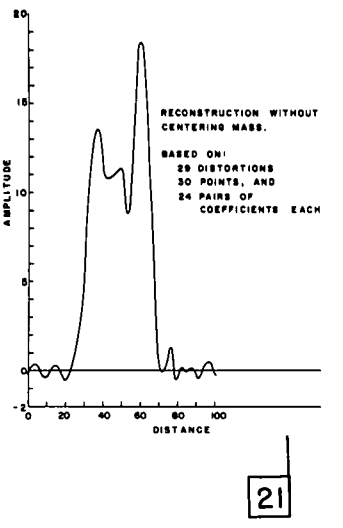

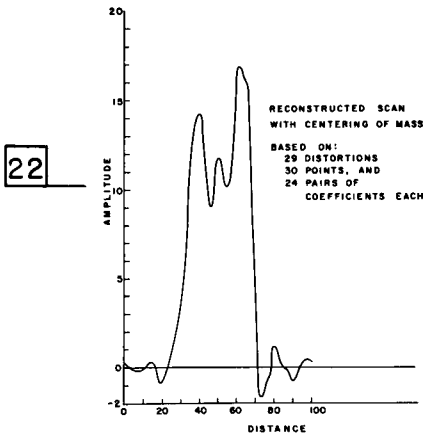

Figures 18 through 22

the nature of the undistorted image. The reduction of information content by the atmospheric turbulence can be visualized by imagining that the essential information which was desired from the image was, how many peaks are present in the image, and secondly what is the relative order of amplitude of the three peaks, i.e., which is largest, which is next largest, and which is smallest.

Before attempting the peak spectrum selection technique, some more common forms of processing were performed. For example, Fig. 19 shows the addition or integration of the twenty-nine distorted waveforms. The result is an image in which the third peak is completely missing. Thus, in terms of the imagined information desired from the image, this type of processing is unsuccessful.

One component of a turbulence distortion can be visualized as a gross shift of the image. It would, therefore, seem reasonable that this shift could cause a considerable loss of information in the process of direct integration previously described. For this reason a second integration was performed, but this time the center of gravity, i.e., the first moment of the flux distribution was determined and all images were shifted to have a common center of gravity prior to integration. Figure 20 shows a result of this second integration. There is no significant improvement associated with this form of processing.

The twenty-nine distortions were then subjected to Fourier analysis with the aid of the GDC 1604 computer and the peak spectrum selection technique was applied. This was first

accomplished without using the center of gravity shift and the results are shown in Fig. 21. The third peak is now present; the three peaks have approximately correct relative amplitudes although considerable distortion still exists. Figure 22 shows the results of applying the peak spectrum selection technique where the phase estimates were made after all images were shifted to common center of gravity. Comparison with Fig. 18 shows that while the restoration of detail is not complete, i.e., it is lacking in contrast, much of the detail of the original image has been recovered.

8.0 TIME INVARIANT DISTORTIONS

8.1 Techniques and Noise Limitations

The preceding section dealt with the case of time variant image distortion, i.e., the situation in which a time sequence of recorded images shows a different distortion in each exposure. Another case of interest is the time invariant distortion in which a time sequence of image recordings shows an identical distortion for each exposure. Lens aberrations would be of this class of distortion. Atmospheric turbulence can also produce this type of distortion, for example, in the case where a long time exposure is required. In a long time exposure a large statistical sample of the turbulence is averaged and there is therefore little variability from image recording to image recording. This type of distortion is

therefore characterized by a transfer function which is temporally invariant. Figure 23 shows a hypothetical transfer function for this type of distortion.

If the transfer function is known, restoration can be accomplished by amplifying each of the spatial frequencies by an amount which exactly compensates for the attenuation which it has suffered. The limitation in quality for this type of restoration lies in the presence of noise. Any real sensor recording an image is ultimately limited by some type of noise. In the example shown in Fig. 23, the noise is assumed to be white or flat with frequency. In the process of amplifying each of the spatial frequencies to compensate for its attenuation, the amplitude of the noise of that spatial frequency will also be amplified by an identical amount. Figure 23 shows the noise spectrum which would result after compensation for the transfer function of that example. A spatial frequency which had an amplitude equal to the noise prior to restoration will have an amplitude equal to noise after restoration. It is conceptually important that the information content of a single image is not increased by any such processing. However, where simple additive noise is the limitation in the restoration, the signal-to-noise ratio can be increased by integration processes well established in the fields of radar and communication.

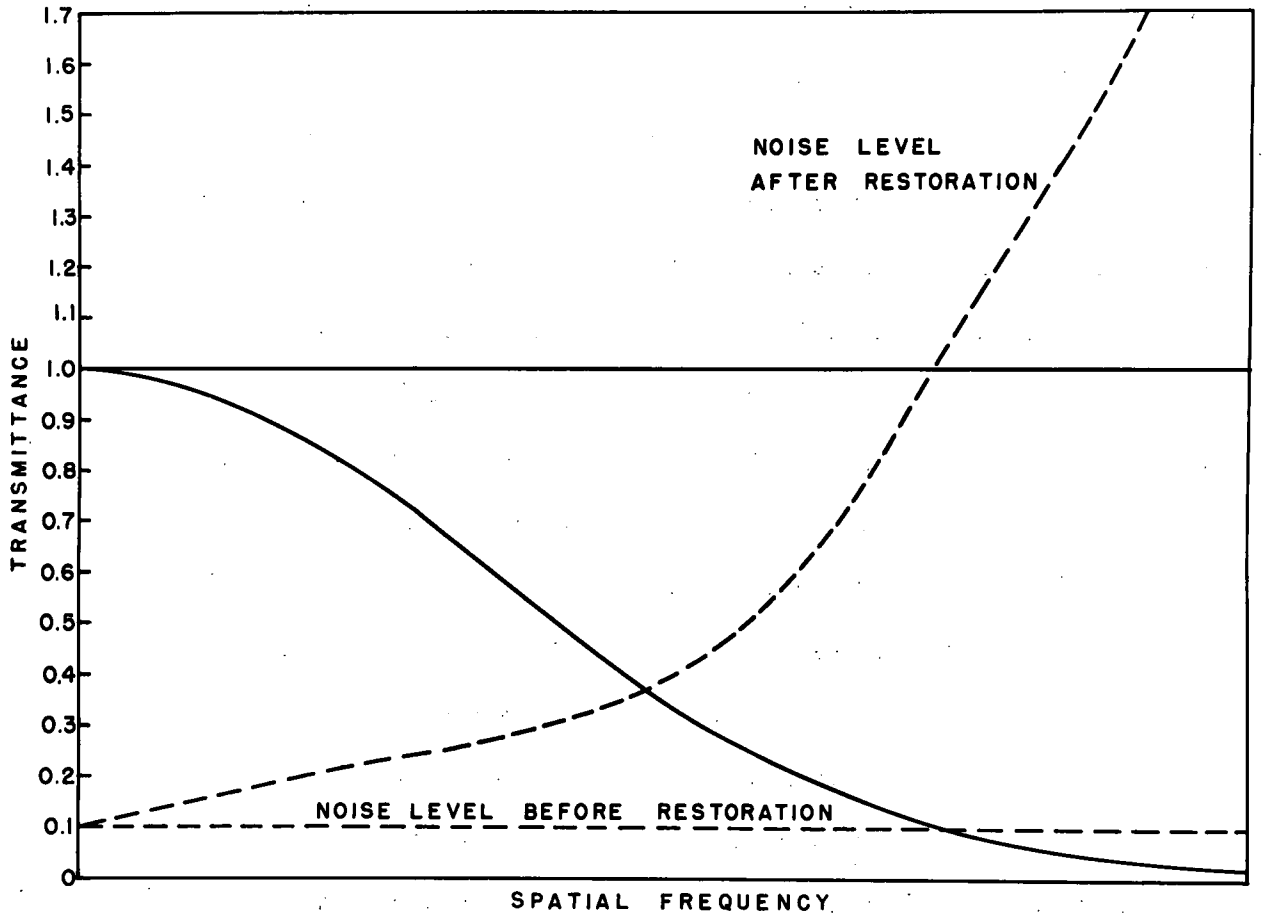

Figure 23 Typical transfer function.

8.2 Processing of Noisy Images

A demonstration of the improvement of signal-to-noise ratio by integration was performed. An image orthicon television chain was used to view a test pattern. The chain was purposely adjusted to give an extremely poor signal-to-noise ratio on the video monitor. The upper left photograph in Fig. 24 shows the photographic recording of a monitor image of a single frame (1/30 second) of the test pattern. As can be seen, the noise level was sufficiently high so that little, if any, information is present in this recorded image. Integration was then accomplished by increasing the exposure time of the camera used to photograph the monitor. For example, the second image shows an exposure time four times that of the first image with the f number of the optical system adjusted to maintain constant integrated flux. The sequence of pictures demonstrates the effect of increasing the number of frames which are averaged or integrated. Figure 24 shows clearly the increase in information content which can be obtained by increasing the period of observation or the number of images which are processed. If it is imagined that the upper left-hand picture representing an exposure of one frame was the image which resulted from the correction of a temporally invariant distortion, then the pictures which follow indicate the improvement in image information which could be obtained as a result of processing of multiple images.

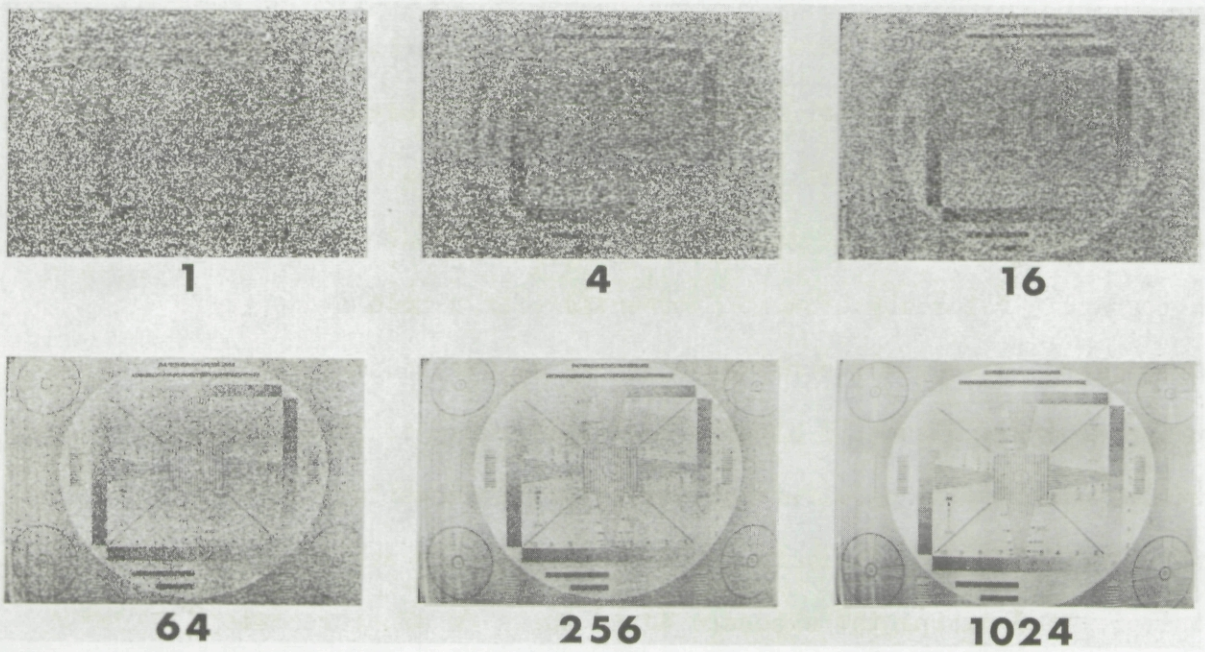

Figure 24 Illustration of the effect of time averaging. The original noise level is 128 times normal image orthicon noise and the number below each picture indicates the number of frames which have been integrated.

8.3 Example of a Time Invariant Restoration

The techniques involved in the restoration of temporally invariant distortions were studied by means of simple mathematical distortions of this class. One example of a temporally invariant distortion is the case of a photograph taken while the object to be photographed is in motion all during the time of the exposure. This would be the equivalent, for example, of a reconnaissance photograph taken under conditions of inadequate image motion compensation. Figure 25 shows a distortion of this type which was mathematically constructed. Here the block letters ARPA were smeared horizontally by an amount which corresponds to an image motion during the exposure equal to 1 1/2 times the width of a block letter. The resulting image distortion is shown in the top of Fig. 25. This distorted image along with information as to the nature of the distortion process were fed into the computer which then performed Fourier analysis of the distorted image, amplification of each of the Fourier components to compensate for their attenuation, and the construction of the restored image which is shown in the bottom of Fig. 25. In this "noiseless case" the image recovery was accurate to the eighth significant figure and was limited only by the extent to which the finite Fourier series could approximate the image in question.

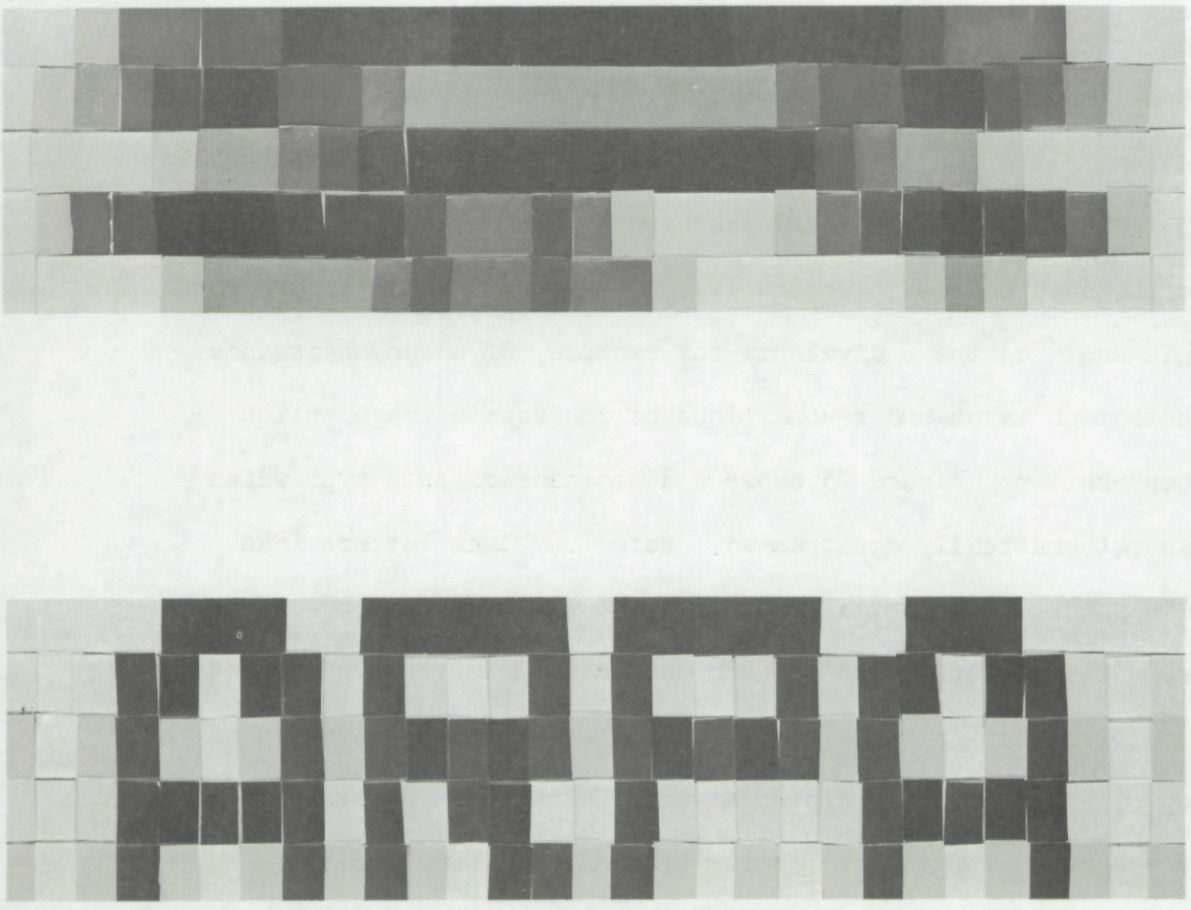

Figure 25 Image distortion and recovery.

9.0 THE FILM SCANNER

The preceding sections have described techniques of image restoration and shown examples of distortions and restorations by means of which these techniques have been explored and proved. It was recognized at an early state in the project that the restoration of atmospheric-turbulence-distorted images by these techniques would require some type of automatic accumulation of input data for the computer. The most easily adapted sensor for recording the distorted images is photographic film. For this reason it was decided that the initial trials of real image restorations would be accomplished from images recorded on photographic film. The number of resolution elements associated with the image distortions virtually prohibits the hand processing of these films in order to obtain input data for the computer. A considerable project effort has therefore been directed toward the construction of a film scanner capable of automatically reducing the input data into computer format.

Figure 26 is a photograph of the completed film scanner and associated electronics. At the left rear of the picture may be seen a projection system through which 16 mm film is fed. Films of 35 mm or 70 mm would be printed on 16 mm format for use in this scanner. Scanner heads to accommodate the larger formats can be constructed if required. The image is projected onto the rectangular, flat, white metal mask (or screen) shown in the middle of the picture. The mask contains a small aperture and the flux passing through the aperture is imaged onto the

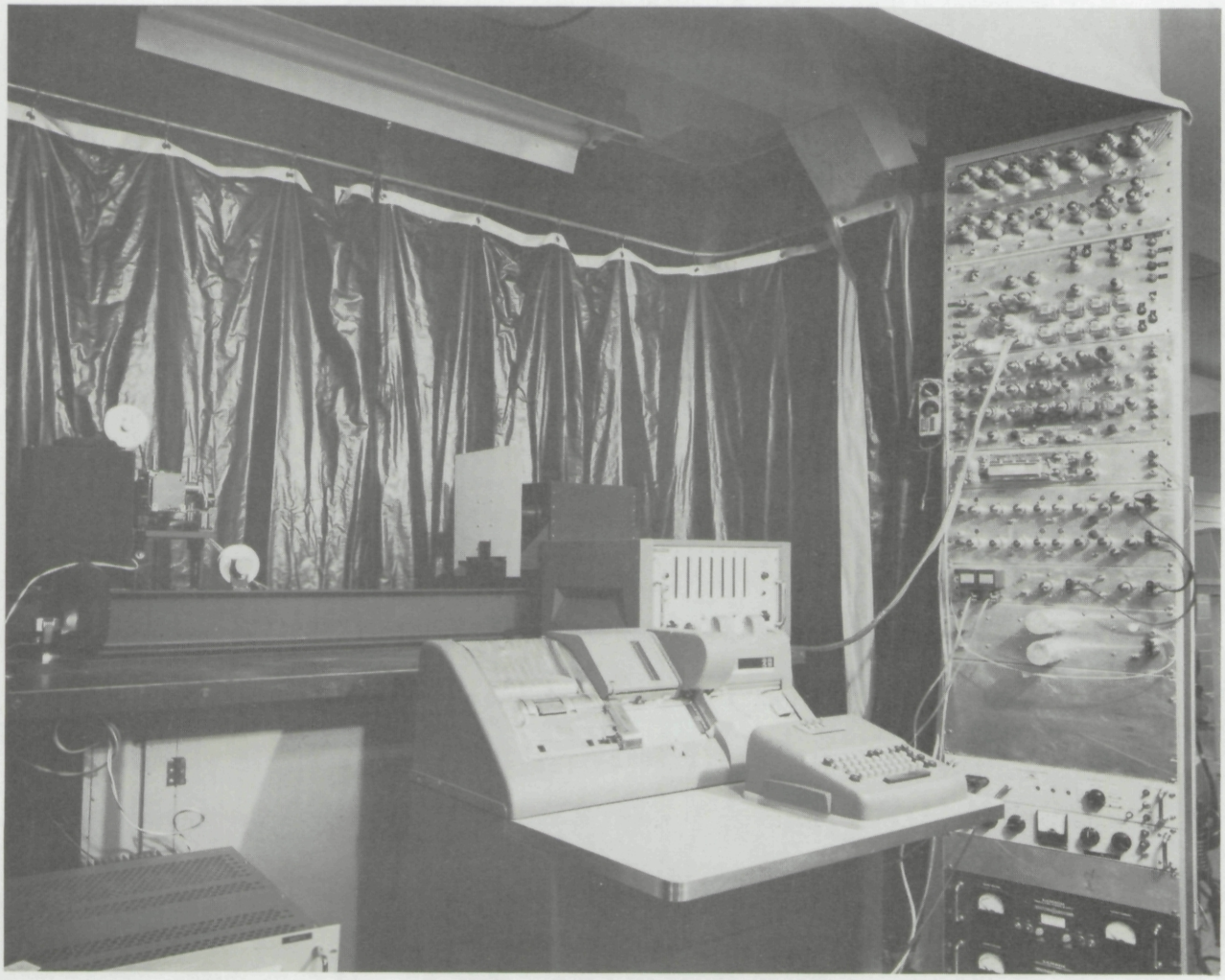

Figure 26 Film scanner (in rear) and associated electronics.

photocathode of a multiplier phototube which is mounted in the black box behind the white mask.

Figure 27 shows a close-up of the projection system. The operation of the system will be explained with the aid of the block diagram shown in Fig. 28. The scanning is accomplished by physical movement of the film in the image plane. A horizontal scan is accomplished in a series of discrete steps. Stepping pulses are supplied by the motor driver unit and activate stepping motors in the projection unit. The horizontal counter counts the number of horizontal steps which have been taken. When the desired number of steps have been accomplished the motor driver unit supplies a series of rapid pulses which cause the stepping motor to retrace to its original position, and at the same time take one vertical step. The horizontal scan is then repeated. When the desired number of vertical steps have been completed, the motor driver supplies a series of rapid pulses to the vertical motor which cause it to retrace to its starting position. The system is now ready for a new film frame.

The output of the multiplier phototube is fed into a voltage-to-frequency converter. The converter output is then counted. The digital output of the counter is serialized so that it may be fed directly to an IBM card punch. The system in this way accomplishes automatic recording on IBM cards of the images contained on the film.

Where commercial units were employed, their identifying trade names and serial numbers are shown on the block diagram. The electronic circuits designed and constructed by the Visibility Laboratory are shown in Figs. 29 through 36.

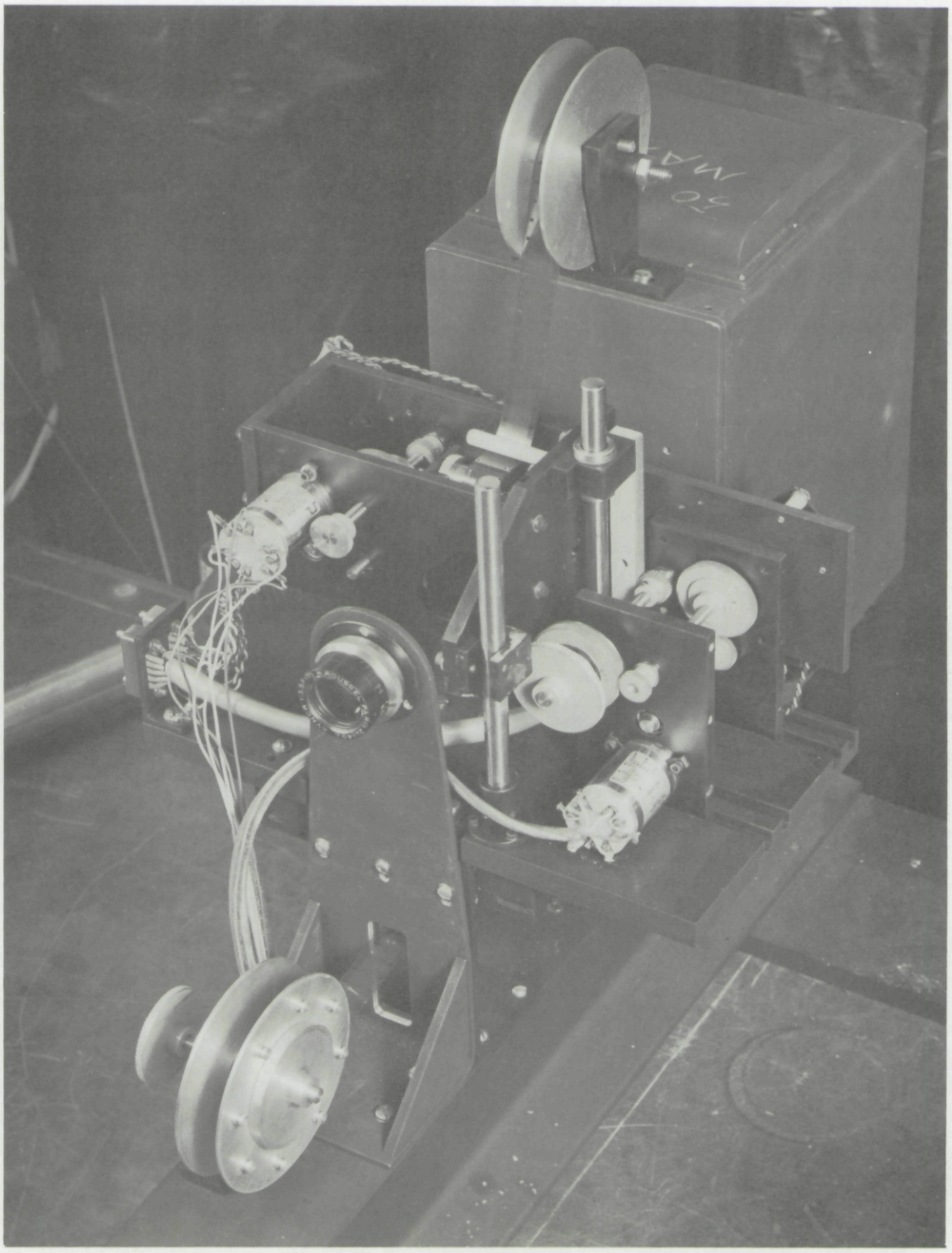

Figure 27 Close-up of film scanner head.

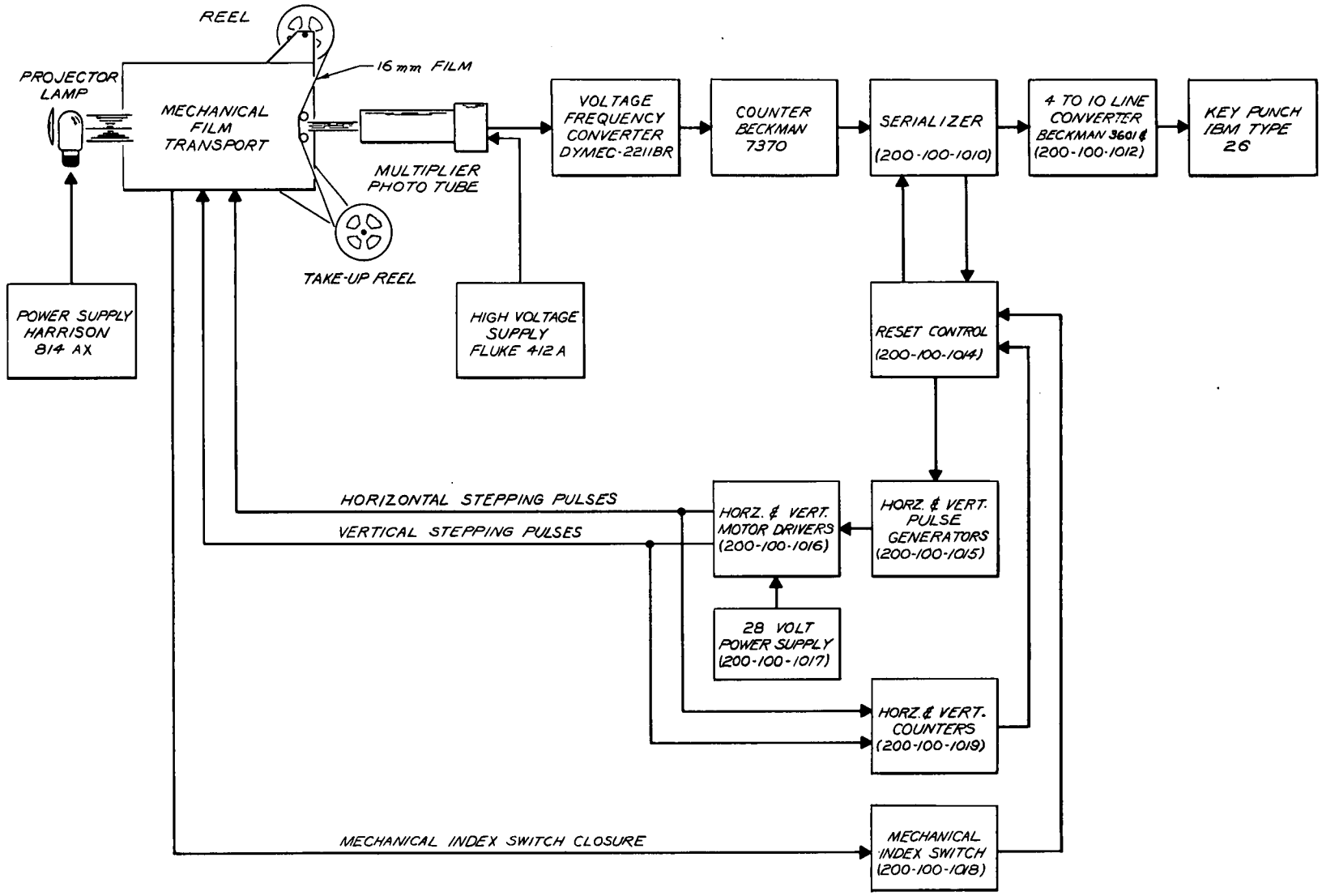

Figure 28 Block diagram scanner system.

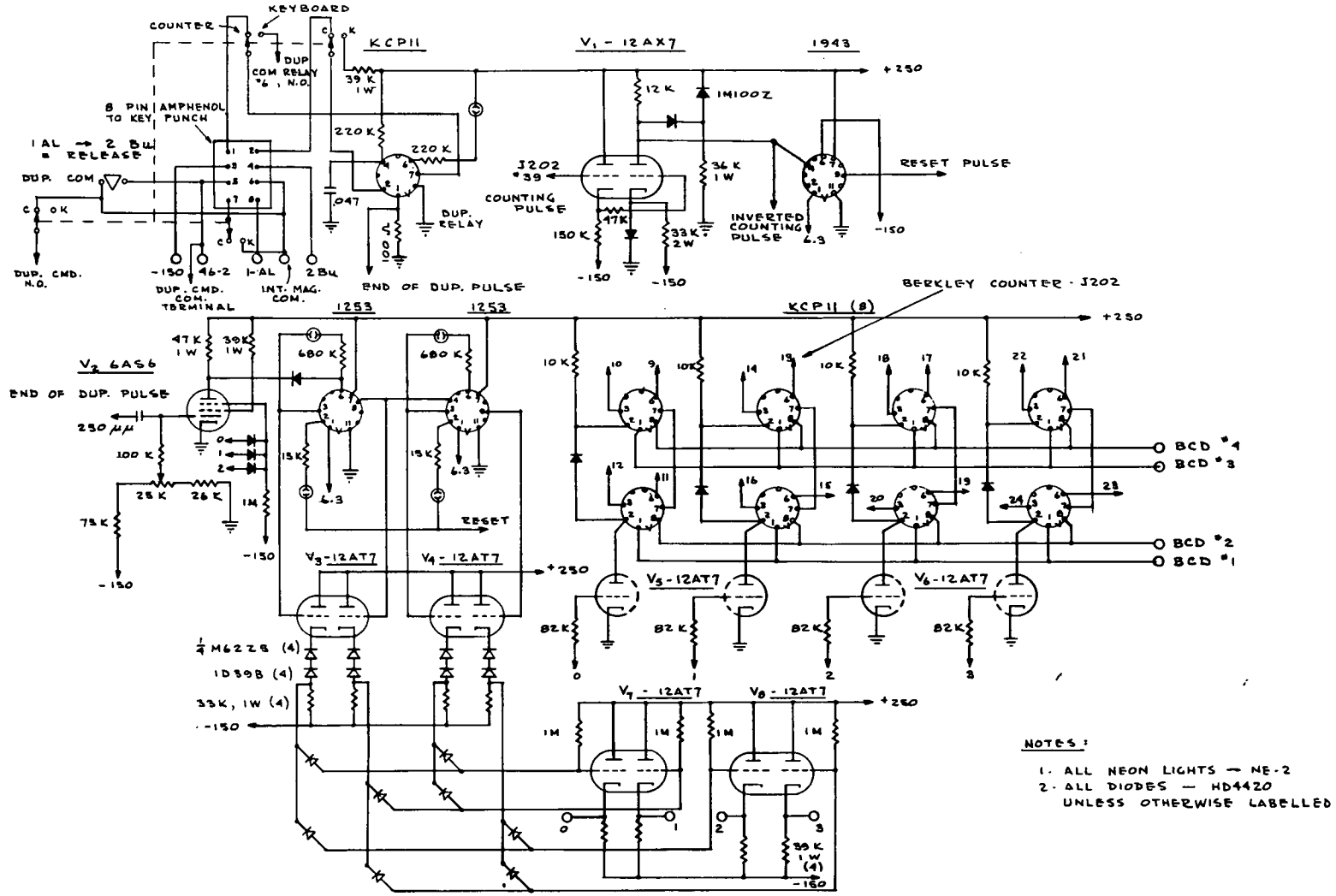

Figure 29 Circuit Diagram – Serializer.

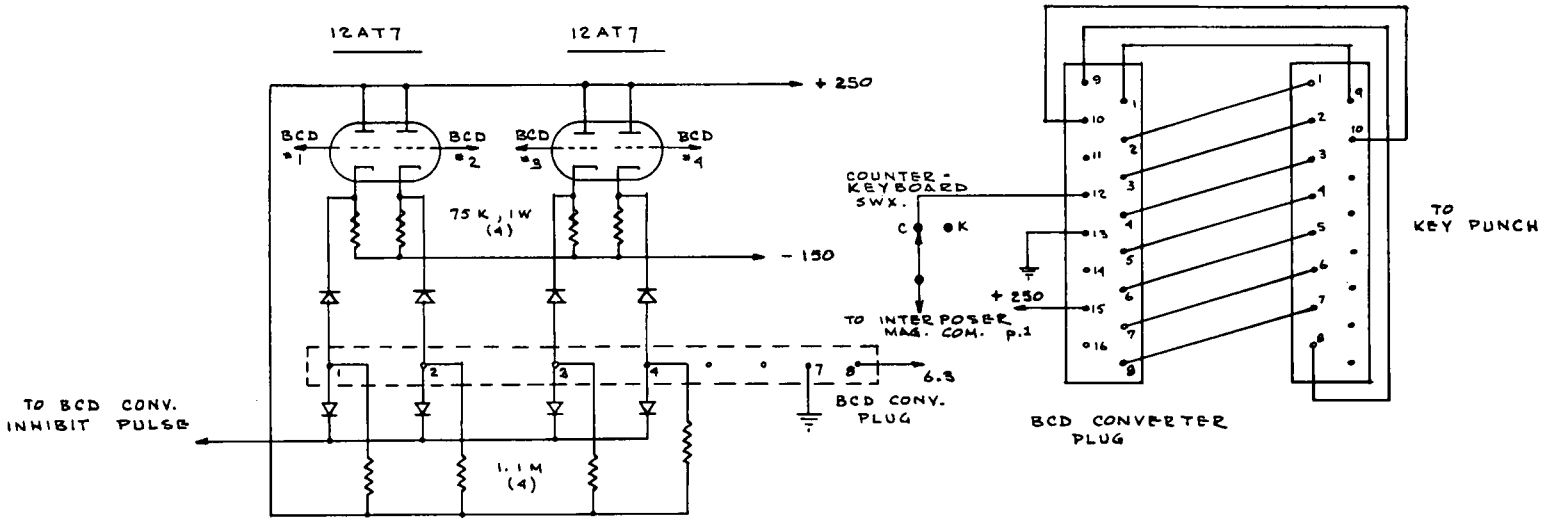

NOTE:

ALL DIODES ARE HD4420
UNLESS OTHERWISE LABELLED

Figure 30 Circuit Diagram - BCD Converter.

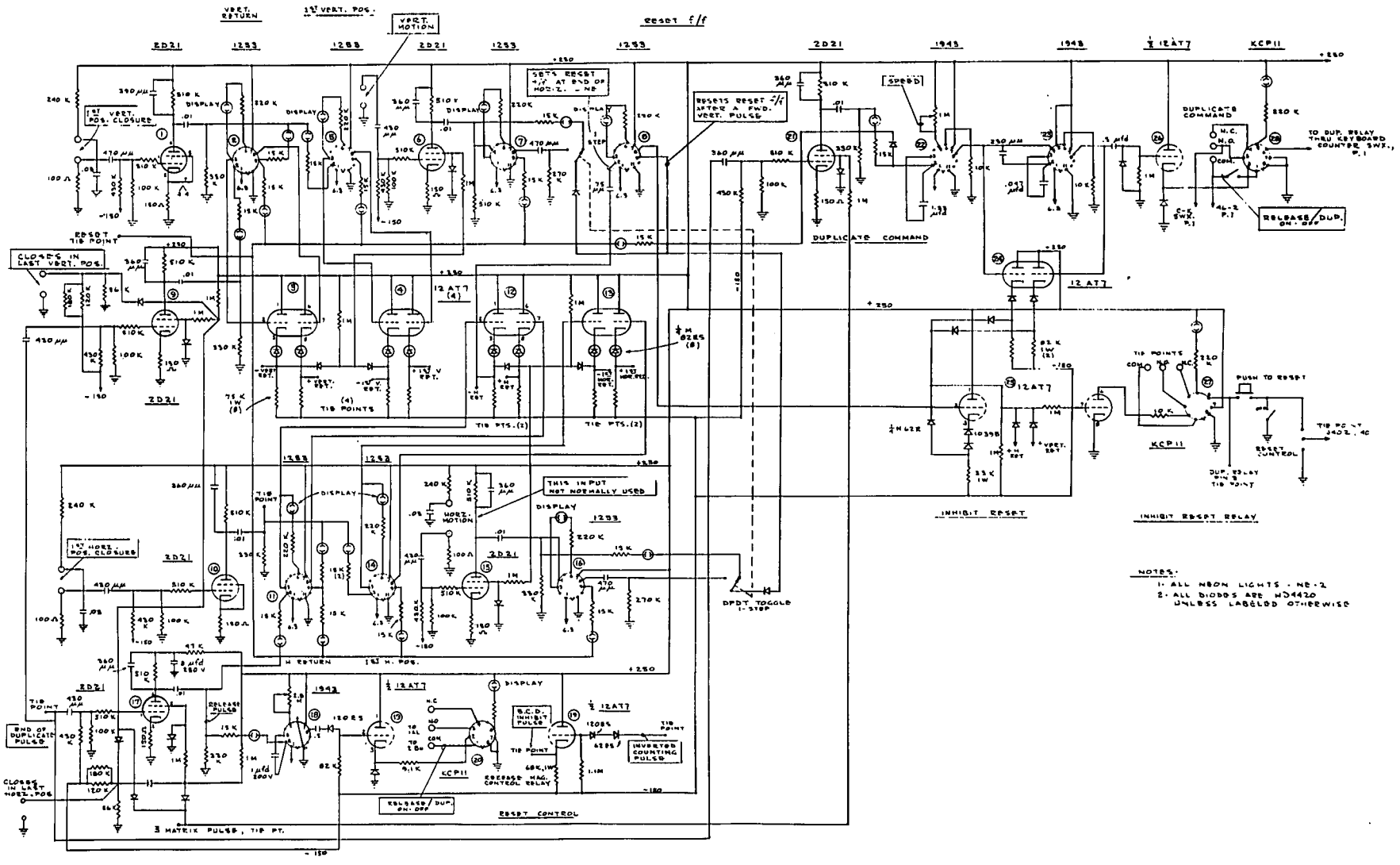

Figure 31 Circuit Diagram – Reset Control.

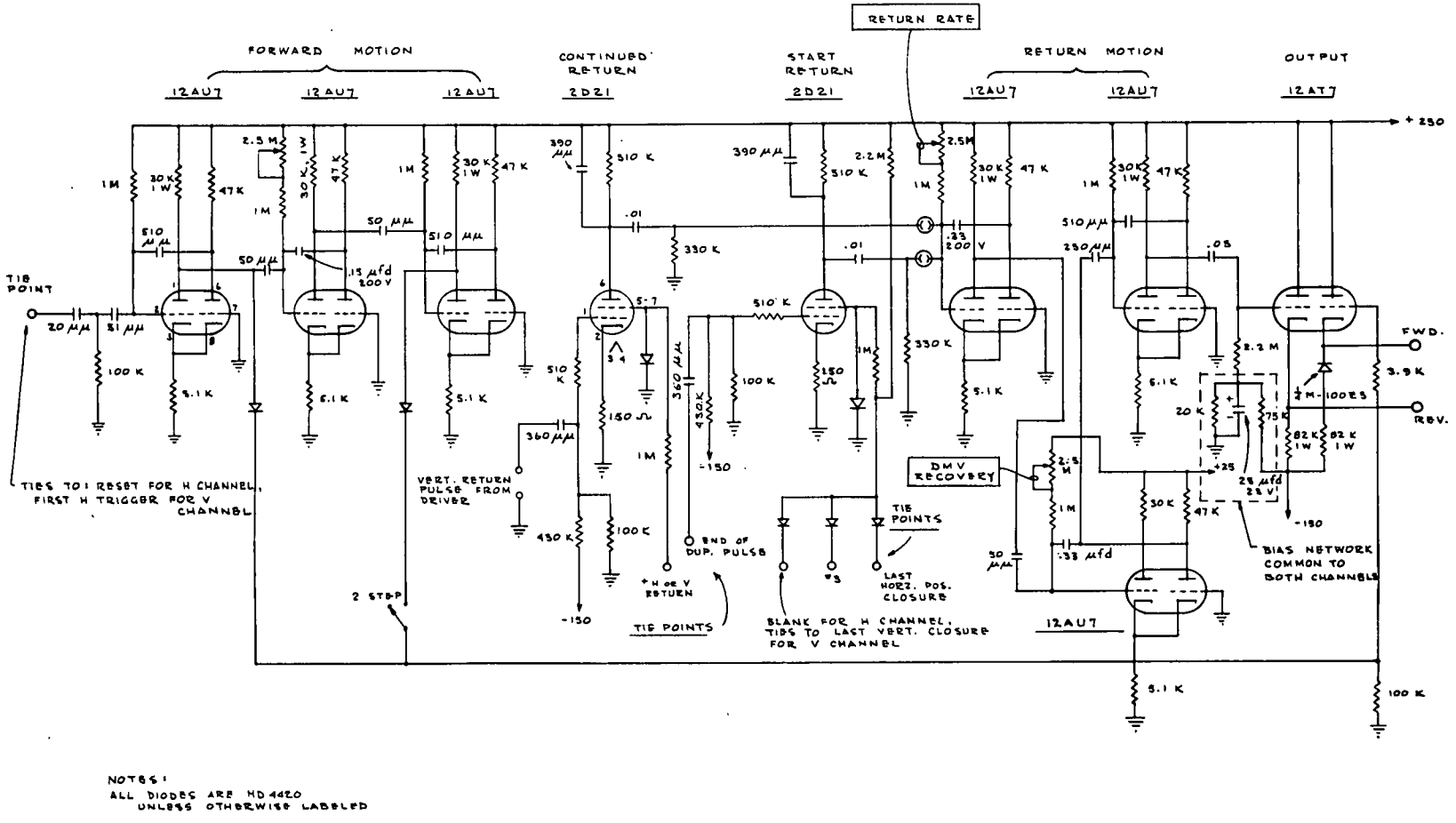

NOTES:
ALL DIODES ARE HD 4420 UNLESS OTHERWISE LABELED

Figure 32 Circuit Diagram — Forward & Reverse Pulse Generator.

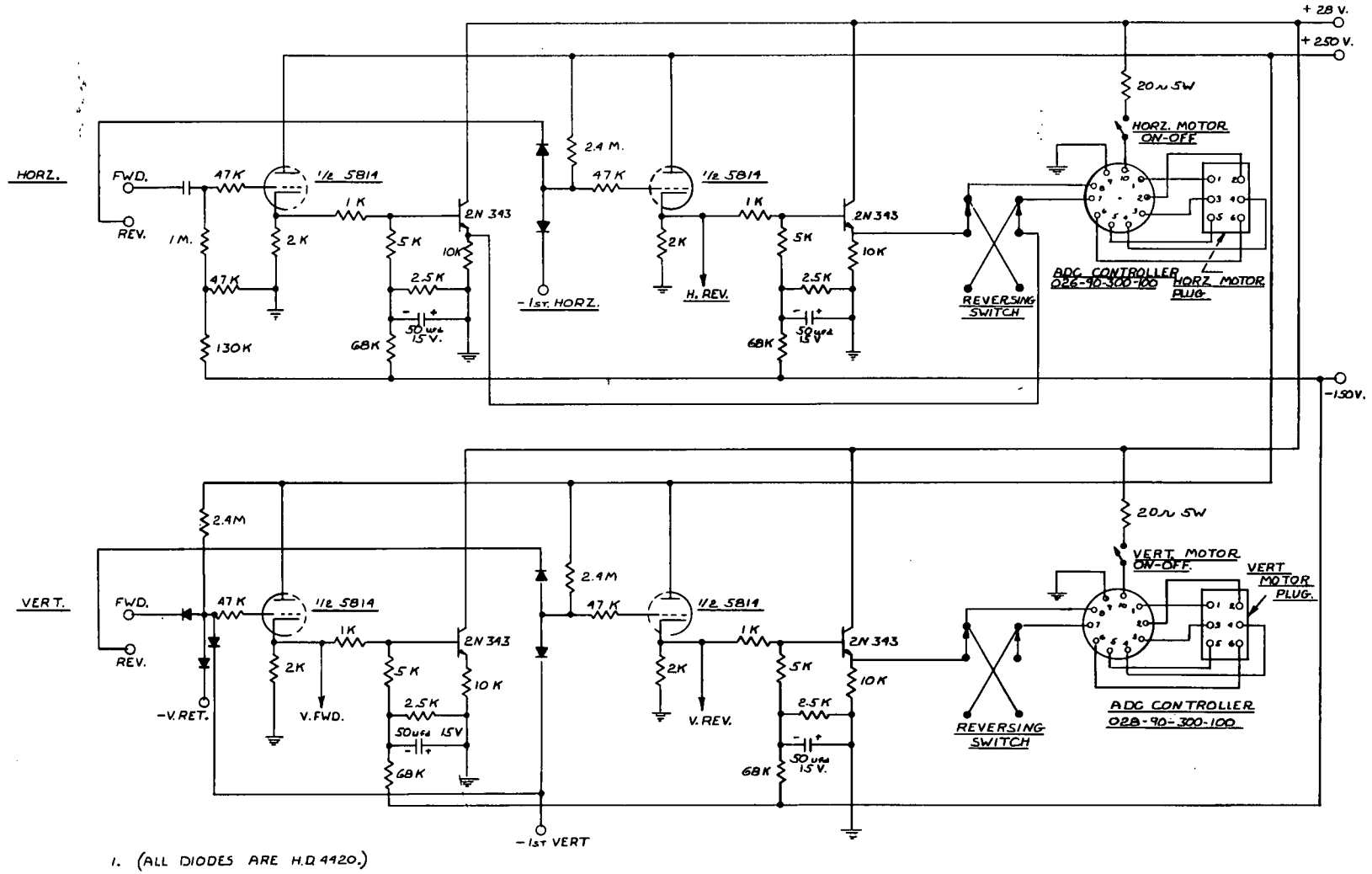

Figure 33 Circuit Diagram — Horizontal & Vertical Motor Control.

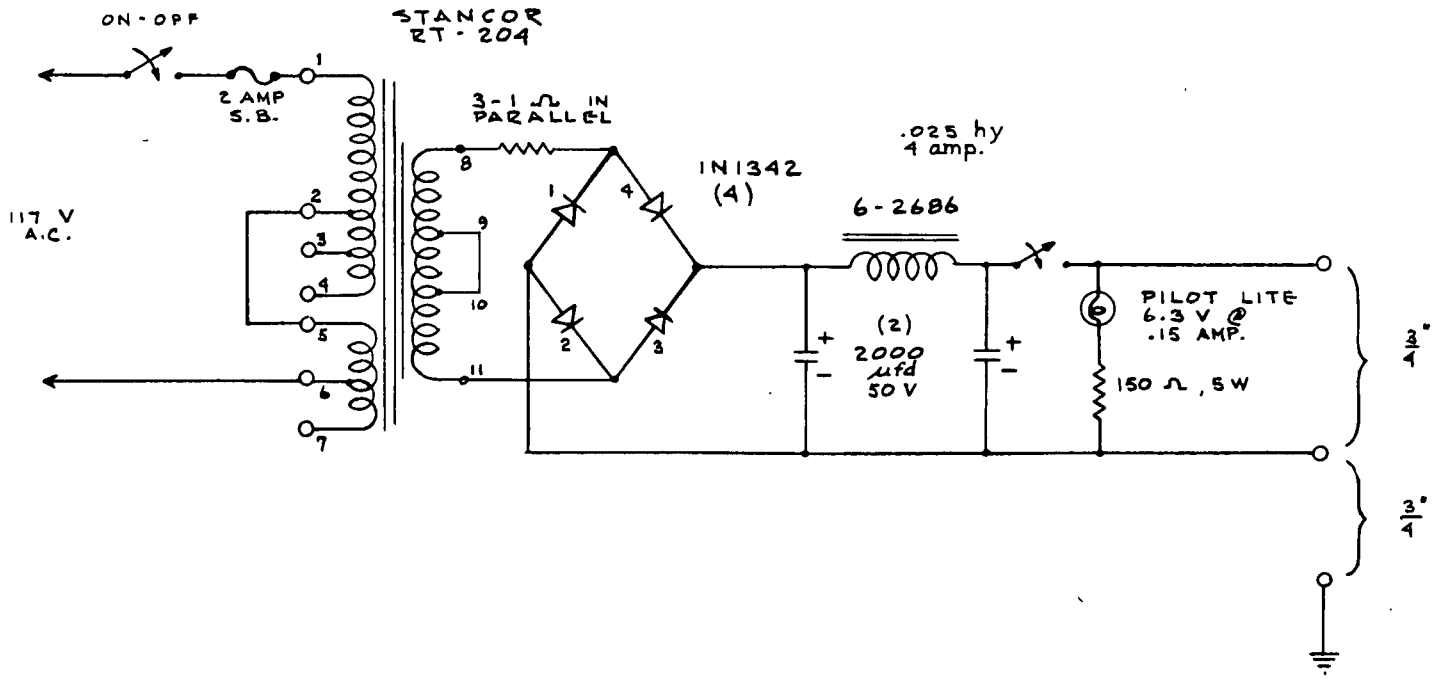

Figure 34 Circuit Diagram – 24 Volt Supply.

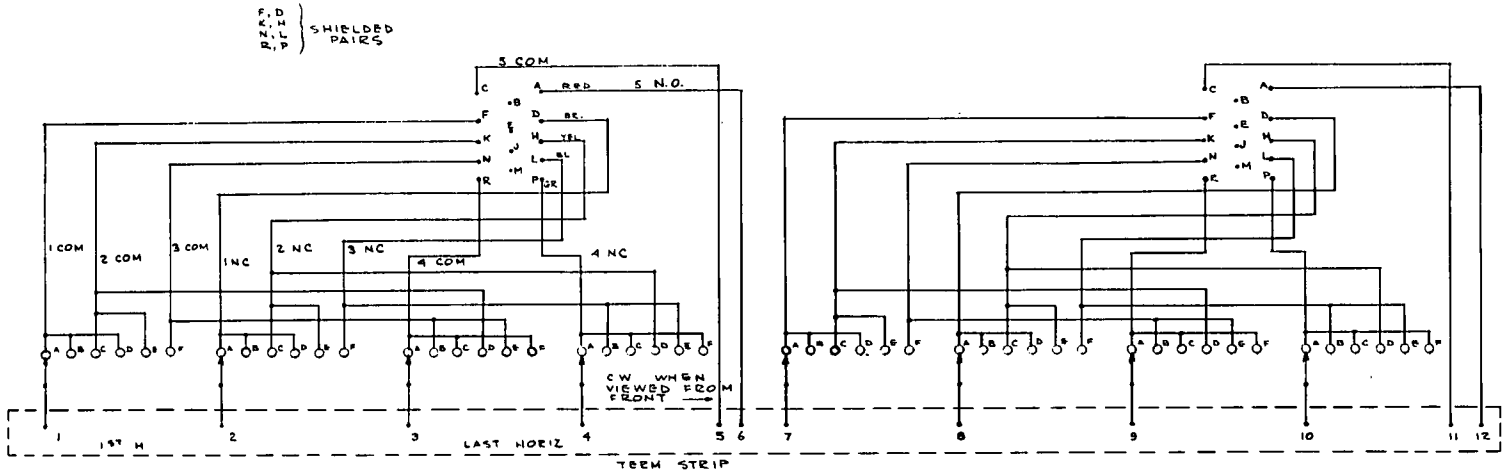

POS.	1ST H		LAST H
A	1	-	4
B	1	-	3
C	2	-	4
D	1	-	2
E	2	-	3
F	3	-	4

	TWISTED PAIR		
5 CAM	BLK	RED	5 N.O.
1 CAM	BLK	BR	1 N.C.
2 CAM	BLK	YBL	2 N.C.
3 CAM	BLK	BL	3 N.C.
4 CAM	BLK	GR	4 N.C.

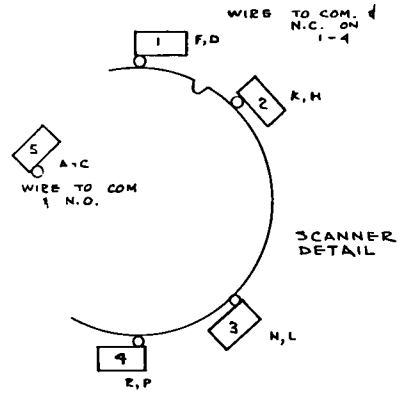

Figure 35 Circuit Diagram – Switch.

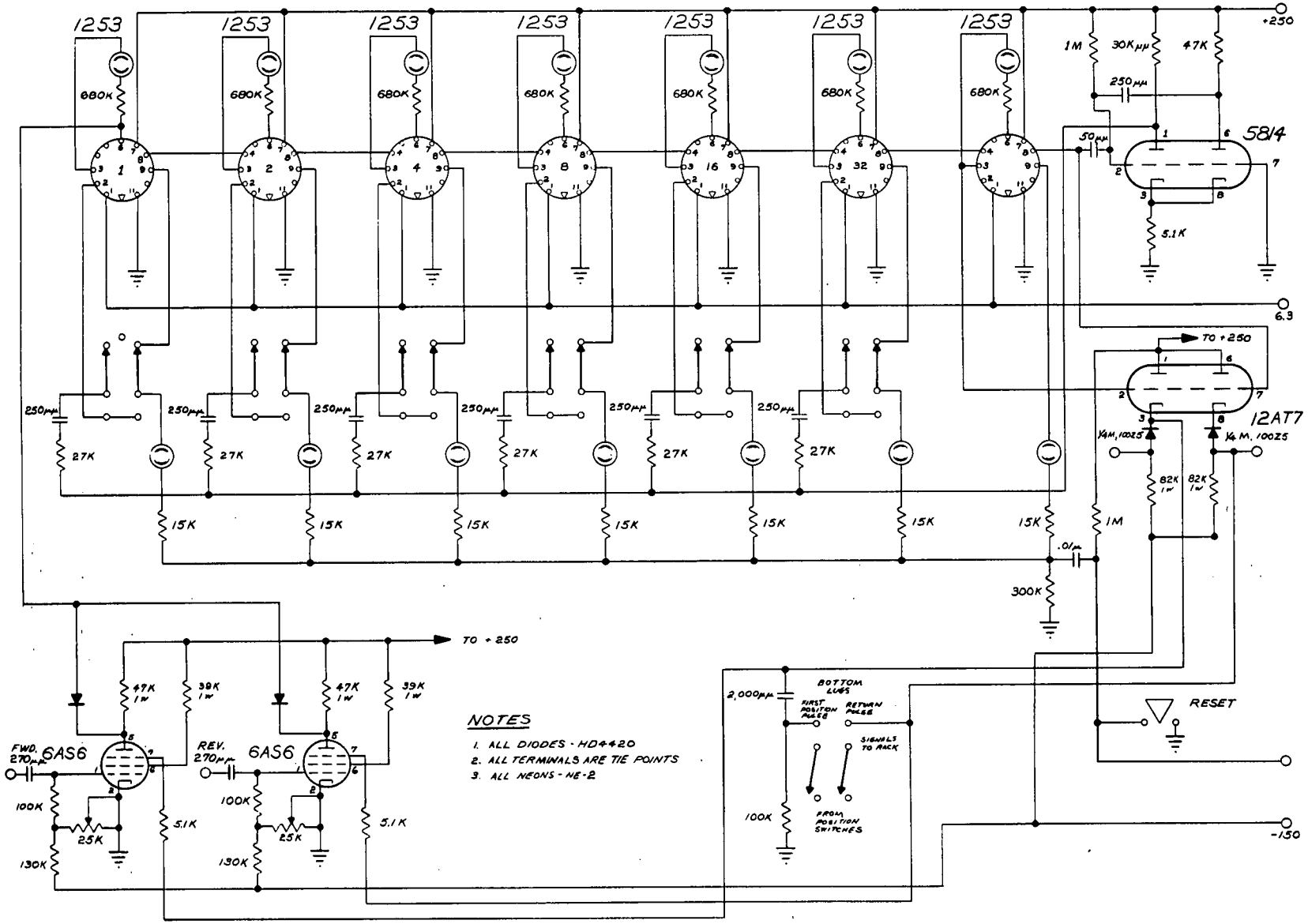

Figure 36 Circuit Diagram – Horizontal & Vertical Counters.

At the time of writing of this report, the construction and assembly of the film scanner system has been completed and effort is presently directed toward the scanning of test films used to check the reliability of the system.

10.0 FUTURE PLANS

The computer program used to accomplish the restoration of the smeared ARPA image has been rewritten to allow for smear in two dimensions. A mathematical distortion of the block letters, ARPA, corresponding to a two-dimensional smear will be fed into the computer as a test of this program. At the same time, photographically recorded two-dimensional smears of the block letters ARPA are being prepared. These are accomplished by masking the entrance pupil of the recording camera to the form of a square and then defocusing the image so that every point in object space becomes a square in the image plane. As in the case of the one-dimensional smear, the smear function will be sufficiently large, such that the block letters ARPA cannot be identified in the distorted images.

Because of the presence of film noise, the restoration of a single distortion from a single film frame may result in an image of very high noise level. For this reason multiple images will be recorded, that is, a sequence of film frames are being prepared, each of which is an identical smear of the block letters ARPA. The computer program will therefore involve not only restoration of each frame but also an integration of the resulting recovered images to form a single image of high signal-to-noise ratio.

When the temporally invariant distortions of this type have been successfully recovered, the next step will be to generate film strips with the optical system used to produce atmospherically distorted images in the laboratory. The flux levels and time exposures will be chosen so as to give large statistical sampling of the turbulence and therefore produce temporally invariant distortions. After these distortions have been successfully processed, additional atmospheric distortions will be generated of the temporally variant variety. These film strips will be scanned and fed into the computer and the two-dimensional version of the peak spectrum selection technique will be used to attempt restorations.

The above trials will represent a checkout of the entire system from the film scanner through the computer programing and will constitute a test of the restoration techniques. When these techniques and the system have been demonstrated to be performing adequately, the system will be ready for attempted restorations of some real space photographs. While the system as presently constructed is inadequate for any volume processing, it should be extremely adequate for demonstrating that image improvement can be obtained by the techniques which have been described. The task of engineering a system capable of operation with an astronomical system should not be initiated until the simple system which has been constructed has clearly demonstrated the feasibility of accomplishing this type of image restoration.

Appendix I.

Derivation of Fourier series on a set of discrete point values.

Section A treats the one-dimensional case and Section B treats the two-dimensional case.

Section A.

Derivation of Fourier series on a one-dimensional set of discrete point values.

This derivation is based on matter found in Introduction to numerical analysis, Hildebrand, McGraw-Hill, 1956, p. 373 ff.

The following determinations will be used later in the derivation.

Known:

$$\sum_{i=0}^{a-1} \cos \frac{2\pi i m}{a} = 0 , \quad m \neq pa \qquad (0.1)$$

$$= a , \quad m = pa \qquad (0.2)$$

Where: a is any integer > 1

p is any integer ≥ 0

$$\sum_{i=0}^{a-1} \sin \frac{2\pi i m}{a} = 0 \qquad (0.3)$$

Evaluate:

$$\sum_{i=0}^{a-1} \cos \frac{2\pi i m}{a} \cos \frac{2\pi i n}{a} =$$

$$= \frac{1}{2} \sum_i \left[\cos \frac{2\pi i (m+n)}{a} + \cos \frac{2\pi i (m-n)}{a} \right] = \varrho \qquad (1)$$

for $\frac{a}{2} \geq m > n \geq 0$

$\frac{a}{2} \geq n > m \geq 0$

} i.e.: $m \neq n$

Then in either of the two last equations:

$$a > m+n > 0 \; ; \quad m-n \neq 0 \; ; \quad \frac{a}{2} \geq m-n \geq -\frac{a}{2}$$

From (0.1): $\varrho = \frac{1}{2}(0+0) = 0 \qquad (1.1)$

For: $\frac{a}{2} > m = n > 0$

$$a > m+n > 0$$

$$m-n = 0$$

From (0.1) and (0.2): $\ell = \frac{1}{2}(0+a) = \frac{a}{2}$ (1.2)

For: $m = n = 0$

$m+n = 0$

$m-n = 0$

From (0.2): $\ell = \frac{1}{2}(a+a) = a$ (1.3)

For: $m = n = \frac{a}{2}$

$m+n = a$

$m-n = 0$

From (0.2): $\ell = \frac{1}{2}(a+a) = a$ (1.4)

Evaluate: $\sum_{i=0}^{a-1} \sin \frac{2\pi i m}{a} \sin \frac{2\pi i n}{a} =$

$= \frac{1}{2} \sum_i \left[\cos \frac{2\pi i (m-n)}{a} - \cos \frac{2\pi i (m+n)}{a} \right] = h$ (2)

For: $\left.\begin{array}{l} \frac{a}{2} \geq m > n \geq 0 \\ \frac{a}{2} \geq n > m \geq 0 \end{array}\right\}$ i.e.: $m \neq n$

Then in either of the two last equations:

$$a > m+n > 0 \; ; \quad m-n \neq 0 \; ; \quad \frac{a}{2} \geq m-n \geq \frac{a}{2}$$

From (0.1): $h = \frac{1}{2}(0+0) = 0$ (2.1)

For: $\frac{a}{2} > m = n > 0$

$$a > m+n > 0$$

$$m-n = 0$$

From (0.2) and (0.1): $h = \frac{1}{2}(a+0) = \frac{a}{2}$ (2.2)

For: $m = n = 0$

$$m+n = 0$$

$$m-n = 0$$

From (0.2): $h = \frac{1}{2}(a - a) = 0$ (2.3)

For: $m = n = \frac{a}{2}$

$m + n = a$

$m - n = 0$

From (0.2): $h = \frac{1}{2}(a - a) = 0$ (2.4)

Evaluate: $\sum_{i=0}^{a-1} \cos \frac{2\pi i m}{a} \sin \frac{2\pi i n}{a} =$ (3)

$$= \frac{1}{2} \sum_i \left[\sin \frac{2\pi i (m+n)}{a} - \sin \frac{2\pi i (m-n)}{a} \right] =$$

$= \frac{1}{2}(0 - 0)$, from (0.3) (3.1)

Evaluate: $\sum_{i=0}^{a-1} \sin \frac{2\pi i m}{a} \cos \frac{2\pi i m}{a} =$ (4)

$$= \frac{1}{2} \sum_i \left[\sin \frac{2\pi i (m+n)}{a} + \sin \frac{2\pi i (m-n)}{a} \right] =$$

$= \frac{1}{2}(0 + 0) = 0$, from (0.3) (4.1)

Assume: $f(x) = \sum_{k=0}^{\frac{a}{2}} \left(A_k \cos \frac{2\pi x k}{L} + B_k \sin \frac{2\pi x k}{L} \right)$

Where L is the length of the period of the function on x.

From Hildebrand: If function is defined at (a+1) equally spaced points the Fourier series will agree exactly with the function at those points if the series contains $\frac{a}{2}$ sets of coefficients in addition to the constant or zero-order term.

a must be even.

Define: $x_i = \frac{i L}{a}$

Then: $\frac{2\pi x_i k}{L} = \frac{2\pi i k}{a}$

$$f(x_i) = \sum_{k=0}^{\frac{a}{2}} \left(A_k \cos \frac{2\pi i k}{a} + B_k \sin \frac{2\pi i k}{a} \right) \qquad (5)$$

Multiplying (5) by $\cos \frac{2\pi i m}{a}$ and summing over the a independent points x_i ; $i = 0, a-1$:

$$\sum_{i=0}^{a-1} f(x_i) \cos \frac{2\pi i m}{a} =$$

$$= \sum_{i=0}^{a-1} \sum_{k=0}^{\frac{a}{2}} \left(A_k \cos \frac{2\pi i k}{a} \cos \frac{2\pi i m}{a} + \right.$$

$$\left. + B_k \sin \frac{2\pi i k}{a} \cos \frac{2\pi i m}{a} \right)$$

Assuming convergence of the Fourier series (Fourier series; Hardy, G.H.; MacMillan, 1944, p. 37 ff. Theory of Fourier series and integrals; Carslaw, H.S.; Dover, third edition, 1930, p. 230 ff.):

$$\sum_{i=0}^{a-1} f(x_i) \cos \frac{2\pi i m}{a} = \sum_{k=0}^{\frac{a}{2}} \sum_{i=0}^{a-1} A_k \cos \frac{2\pi i k}{a} \cos \frac{2\pi i m}{a} +$$

$$\left. + B_k \sin \frac{2\pi i k}{a} \cos \frac{2\pi i m}{a} \right)$$

B_k terms vanish throughout, from (4.1).

When $k \neq m$ all terms vanish, from (1.1)

When $k = m = 0$:

$$\Sigma_i f(x_i) \cos \frac{2\pi i \, 0}{a} = A_0 \cdot a \; ; \text{ from (1.3)}$$

$$\boxed{A_0 = \frac{1}{a} \sum_{i=0}^{a-1} f(x_i)}$$

When $k = m = \frac{a}{2}$:

$$\Sigma_i f(x_i) \cos \frac{2\pi i a}{2a} = A_{\frac{a}{2}} \cdot a \; ; \text{ from (1.4)}$$

$$\boxed{A_{\frac{a}{2}} = \frac{1}{a} \sum_{i=0}^{a-1} f(x_i) \cos \pi i}$$

Note: $\cos \pi i = (-1)^i$

When $\frac{a}{2} > k = m > 0$:

$$\Sigma_i f(x_i) \cos \frac{2\pi i k}{a} = A_k \cdot \frac{a}{2} \text{ ; from (1.2)}$$

$$\boxed{A_k = \frac{2}{a} \sum_{i=0}^{a-1} f(x_i) \cos \frac{2\pi i k}{a}}$$

Multiplying (5) by $\sin \frac{2\pi i m}{a}$; summing over the a independent points x_i ; $i = 0, a-1$ and transposing the summation operators as above, since convergence is assumed:

$$\sum_{i=0}^{a-1} f(x_i) \sin \frac{2\pi i m}{a} =$$

$$= \sum_{k=0}^{\frac{a}{2}} \sum_{i=0}^{a-1} \left(A_k \cos \frac{2\pi i k}{a} \sin \frac{2\pi i m}{a} + \right.$$

$$\left. + B_k \sin \frac{2\pi i k}{a} \sin \frac{2\pi i m}{a} \right)$$

A_k terms vanish throughout, from (3.1).

When $k \neq m$ all terms vanish, from (2.1).

When $\frac{a}{2} > k = m > 0$:

$$\Sigma_i f(x_i) \sin \frac{2\pi i k}{a} = B_k \cdot \frac{a}{2} \text{ ; from (2.2)}$$

$$\boxed{B_k = \frac{2}{a} \sum_{i=0}^{a-1} f(x_i) \sin \frac{2\pi i k}{a}}$$

When $k = m = 0$:

$$\Sigma_i f(x_i) \sin \frac{2\pi i 0}{a} = B_0 \cdot 0 \text{ , from (2.3).}$$

$$B_0 = \frac{0}{0}$$

When $k = m = \frac{a}{2}$

$$\Sigma_i f(x_i) \sin \frac{2\pi i a}{2a} = B_{\frac{a}{2}} \cdot 0 \text{ ; from (2.4).}$$

$$B_{\frac{a}{2}} = \frac{0}{0}$$

Although the last two cases are indeterminate, they can be considered as non-existent, since even if they have value they would have no effect, at the points x_i, on the value of $f(x_i)$. The multipliers of B_0 and $B_{\frac{a}{2}}$ in (5) are respectively $\sin \frac{2\pi i 0}{a}$ and $\sin \frac{2\pi i a}{2a}$, both of value 0.

Section B.

Derivation of Fourier series on a two-dimensional set of discrete point values.

As in Section A this derivation is based on Hildebrand.

The following determinations will be used later in the derivation:

Known:

$$\sum_{i=0}^{a-1} \cos\frac{2\pi i m}{a} \cos\frac{2\pi i n}{a} = 0;\ m \neq n \qquad (1.1)$$

$$= \frac{a}{2};\ m = n \neq 0, \frac{a}{2} \qquad (1.2)$$

$$= a;\ m = n = 0, \frac{a}{2} \qquad (1.3)$$

$$\sum_{i=0}^{a-1} \sin\frac{2\pi im}{a} \sin\frac{2\pi in}{a} = 0;\ m \neq n \qquad (2.1)$$

$$= \frac{a}{2};\ m = n \neq 0 \text{ or } \frac{a}{2} \qquad (2.2)$$

$$= 0;\ m = n = 0 \text{ or } \frac{a}{2} \qquad (2.3)$$

$$\sum_{i=0}^{a-1} \sin\frac{2\pi im}{a} \cos\frac{2\pi in}{a} = 0 \qquad (3)$$

Define: $x_k = \frac{k L_x}{P}$; $k = 0, P$

$$\theta_k = \frac{2\pi x_k}{L_x} = \frac{2\pi k}{P}$$

Define: $y_l = \frac{l L_y}{q}$; $l = 0, q$

$$\phi_l = \frac{2\pi y_l}{L_y} = \frac{2\pi l}{q}$$

Where L_x is the length of the period of the function on x and L_y is the length of the period on y.

p and q are the numbers of independent points on x and y at which the function is defined. Total points on x and y are (p+1) and (q+1).

Expanding $f(\theta,\phi)$ with respect to θ:

$$f(\theta,\phi) = \sum_{i=0}^{\frac{p}{2}} \left[A_i(\phi)\cos i\theta + B_i(\phi)\sin i\theta\right]$$

Expanding $A_i(\phi)$ and $B_i(\phi)$:

$$A_i(\phi) = \sum_{j=0}^{\frac{q}{2}} \left[C_{ij}\cos j\phi + D_{ij}\sin j\phi\right]$$

$$B_i(\phi) = \sum_{j=0}^{\frac{q}{2}} \left[E_{ij}\cos j\phi + F_{ij}\sin j\phi\right]$$

Then: $f(\theta_k,\phi_l) = \sum_{i=0}^{\frac{p}{2}} \sum_{j=0}^{\frac{q}{2}} \left(C_{ij}\cos i\theta_k \cos j\phi_l + \right.$

$$+ D_{ij}\cos i\theta_k \sin j\phi_l + E_{ij}\sin i\theta_k \cos j\phi_l +$$

$$\left. + F_{ij}\sin i\theta_k \sin j\phi_l\right) \qquad (4)$$

To show that this function represents the variously oriented

sin and cos waveforms, the function can be written:

$$f(\theta_k, \phi_1) = \frac{1}{2} \sum_{i=0}^{\frac{p}{2}} \sum_{j=0}^{\frac{q}{2}} \left[(C_{ij} - F_{ij}) \cos(i\theta_k + j\phi_1) + \right.$$

$$+ (C_{ij} + F_{ij}) \cos(i\theta_k - j\phi_1) +$$

$$+ (D_{ij} + E_{ij}) \sin(i\theta_k + j\phi_1) +$$

$$\left. + (-D_{ij} + E_{ij}) \sin(i\theta_k - j\phi_1) \right]$$

To determine C_{ij} multiply (4) by $(\cos m\theta_k \cos n\phi_1)$ and sum over the p and q independent x and y axis points:

$$\sum_{k=0}^{p-1} \sum_{1=0}^{q-1} f(\theta_k, \phi_1) \cos m\theta_k \cos n\phi_1 =$$

$$= \sum_{i=0}^{\frac{p}{2}} \sum_{j=0}^{\frac{q}{2}} \sum_{k=0}^{p-1} \sum_{1=0}^{q-1} C_{ij} \cos i\theta_k \cos m\theta_k \cos j\phi_1 \cos n\phi_1$$

All other terms vanish since they contain a summation of sin-cos terms and the summation results in 0, from (3).

The above equation has value only where $i = m$ and $j = m$ simultaneously, from (1.1)

$$\Sigma_k \Sigma_l f(\theta_k, \phi_l) \cos i\theta_k \cos j\phi_l =$$

$$= \Sigma_k \Sigma_l C_{ij} \cos^2 i\theta_k \cos^2 j\phi_l$$

$$C_{ij} = \frac{\Sigma_k \Sigma_l f(\theta_k, \phi_l) \cos i\theta_k \cos j\phi_l}{\Sigma_k \Sigma_l \cos^2 i\theta_k \cos^2 j\phi_l} = \frac{F_c}{G_c}$$

When $i \neq 0, \frac{p}{2}$ and $j \neq 0, \frac{q}{2}$, from (1.2):

$$G_c = \frac{pq}{4} \quad \text{and} \quad C_{ij} = \frac{4}{pq} F_c$$

When $i = 0$ or $\frac{p}{2}$ and $j \neq 0$ or $\frac{q}{2}$

or $i \neq 0$ or $\frac{p}{2}$ and $j = 0$ or $\frac{q}{2}$, from (1.2), (1.3)

$$G_c = \frac{pq}{2} \quad \text{and} \quad C_{ij} = \frac{2}{pq} F_c$$

When $i = 0$ or $\frac{p}{2}$ and $j = 0$ or $\frac{q}{2}$, from (1.3)

$$G_c = pq \quad \text{and} \quad C_{ij} = \frac{1}{pq} F_c$$

To determine D_{ij} multiply (4) by $\cos m\theta_k \sin n\phi_1$ and sum:

$$\Sigma_k \Sigma_1 f(\theta_k, \phi_1) \cos m\theta_k \sin n\phi_1 =$$

$$= \Sigma_i \Sigma_j \Sigma_k \Sigma_1 D_{ij} \cos i\theta_k \cos m\theta_k \sin j\phi_1 \sin n\phi_1$$

with value where $i = m$ and $j = n \neq 0, \frac{q}{2}$ from (2.2):

$$D_{ij} = \frac{\Sigma_k \Sigma_1 f(\theta_k, \phi_1) \cos i\theta_k \sin j\phi_1}{\Sigma_k \Sigma_1 \cos^2 i\theta_k \sin^2 j\phi_1} = \frac{F_d}{G_d}$$

When $i \neq 0$ or $\frac{p}{2}$ and $j \neq 0, \frac{q}{2}$, from (1.2), (2.2)

$$G_d = \frac{pq}{4} \quad \text{and} \quad D_{ij} = \frac{4}{pq} F_d$$

When $i = 0$ or $\frac{p}{2}$ and $j \neq 0$ or $\frac{q}{2}$

$$G_d = \frac{pq}{2} \quad \text{and} \quad D_{ij} = \frac{2}{pq} F_d$$

To determine E_{ij} multiply (4) by $\sin m\theta_k \cos n\phi_1$ and sum:

$$\Sigma_k \Sigma_1 f(\theta_k,\phi_1) \sin m\theta_k \cos n\phi_1 =$$

$$= \Sigma_i \Sigma_j \Sigma_k \Sigma_1 E_{ij} \sin i\theta_k \sin m\theta_k \cos j\phi_1 \cos n\phi_1$$

with value where $i = m \neq 0$ or $\frac{p}{2}$ and $j = n$, from (2.2)

$$E_{ij} = \frac{\Sigma_k \Sigma_1 f(\theta_k,\phi_1) \sin i\theta_k \cos j\phi_1}{\Sigma_k \Sigma_1 \sin^2 i\theta_k \cos^2 j\phi_1} = \frac{F_e}{G_e}$$

When $i \neq 0$ or $\frac{p}{2}$ and $j \neq 0$ or $\frac{q}{2}$, from (1.2), (2.2)

$$G_e = \frac{pq}{4} \quad \text{and} \quad E_{ij} = \frac{4}{pq} F_e$$

When $i \neq 0$ or $\frac{p}{2}$ and $j = 0$ or $\frac{q}{2}$, from (1.3), (2.2)

$$G_e = \frac{pq}{2} \quad \text{and} \quad E_{ij} = \frac{2}{pq} F_e$$

To determine F_{ij} multiply (4) by $\sin m\theta_k \sin n\phi_l$ and sum:

$$\Sigma_k \Sigma_l f(\theta_k, \phi_l) \sin m\theta_k \sin n\phi_k =$$

$$= \Sigma_i \Sigma_j \Sigma_k \Sigma_l f(\theta_k, \phi_l) \sin i\theta_k \sin m\theta_k \sin j\phi_l \sin n\phi_l$$

With value where $i = m \neq 0, \frac{p}{2}$ and $j = n \neq 0, \frac{q}{2}$,

From (2.2):

$$F_{ij} = \frac{\Sigma_k \Sigma_l f(\theta_k, \phi_l) \sin i\theta_k \sin j\phi_l}{\Sigma_k \Sigma_l \sin^2 i\theta_k \sin^2 j\phi_l} = \frac{F_f}{G_f}$$

When $i = m \neq 0$ or $\frac{p}{2}$ and $j = n \neq 0$ or $\frac{q}{2}$, from (2.2):

$$G_F = \frac{pq}{4} \quad \text{and} \quad F_{ij} = \frac{4}{pq} F_f$$

William Hadley Richardson

Appendix II.

Derivation of equations for the transfer function of a diffraction limited optical system.

Assume that a diffraction limited optical system is imaging an infinitely distant, monochromatic point source. The plane electromagnetic wave incident on the entrance pupil, in the absence of turbulence, can be described by the equation

$$a = A \sin(\omega t + \phi). \tag{II-1}$$

Suppose, however, that in the neighborhood of the entrance pupil, the plane wave passed through a thin lamina having a spatially varying index of refraction. The emerging wavefront would then have the form

$$a(x,y) = A(x,y) \sin[\omega t + \phi(x,y)] \tag{II-2}$$

where x and y are the horizontal and vertical directions in the plane of the entrance pupil. This phase disturbance will result in an image distortion, a mathematical derivation of which will now be developed.

The nature of the image can be determined by the application of Huygen's principle in which each point on the wavefront will be considered to be an isotropic radiator. The propagation in a direction (α,β) will then be examined, where α and β are angles measured with respect to the x and y axes respectively.

The optical system would produce an intensity map as a function of α and β such that the intensity is proportional to the square of the amplitude of the vector sum over the wavefront in a plane inclined at the angle (α, β). The constant of proportionality involves the geometry of the optical system and is not relevant to this particular derivation.

For the application of interest, the objects to be imaged have angular subtense on the order of seconds of arc, and the sine and tangent functions may be represented by the angle expressed in radians. Using the central axis as a reference, a point x,y on the wavefront will have a path length increase in the inclined plane relative to the point o,o of

$$\Delta d = \alpha x + \beta y \tag{II-3}$$

This increased path length results in a phase shift relative to the entrance pupil of

$$\gamma = \frac{\alpha x + \beta y}{\lambda} \tag{II-4}$$

Equation (II-2) can therefore be rewritten for the case of propagation in the direction (α, β) as,

$$a(\alpha, \beta, x, y) = A(x,y) \sin\left[\omega t + \frac{\alpha x}{\lambda} + \frac{\beta y}{\lambda} + \phi(x,y)\right] \tag{II-5}$$

The square of the amplitude of the vector sum of Eq. (II-5) over all x and y within the limits of the entrance pupil will be proportional to the intensity of the image at the point corresponding to the direction (α, β).

The image plane intensity is therefore

$$I = \left\{ \int_{-\infty}^{\infty} \int_{-\infty}^{\infty} A(x,y) \cos\left[\frac{\alpha x}{\lambda} + \frac{\beta y}{\lambda} + \phi(x,y)\right] dx\,dy \right\}^2 + \tag{II-6}$$

$$+ \left\{ \int_{-\infty}^{\infty} \int_{-\infty}^{\infty} A(x,y) \sin\left[\frac{\alpha x}{\lambda} + \frac{\beta y}{\lambda} + \phi(x,y)\right] dx\,dy \right\}^2$$

where A(x,y) is zero in the region of x,y outside the boundary of the entrance pupil. By recognizing the concept of dummy variables of integration, (II-6) can be rewritten as

$$I = \int_{-\infty}^{\infty} \int_{-\infty}^{\infty} A(x,y) \cos\left[\frac{\alpha x}{\lambda} + \frac{\beta y}{\lambda} + \phi(x,y)\right] dx\,dy \cdot$$

$$\cdot \int_{-\infty}^{\infty} \int_{-\infty}^{\infty} A(w,z) \cos\left[\frac{\alpha w}{\lambda} + \frac{\beta z}{\lambda} + \phi(w,z)\right] dw\,dz + \tag{II-7}$$

$$+ \int_{-\infty}^{\infty} \int_{-\infty}^{\infty} A(x,y) \sin\left[\frac{\alpha x}{\lambda} + \frac{\beta y}{\lambda} + \phi(x,y)\right] dx\,dy \cdot$$

$$\cdot \int_{-\infty}^{\infty} \int_{-\infty}^{\infty} A(w,z) \sin\left[\frac{\alpha w}{\lambda} + \frac{\beta z}{\lambda} + \phi(w,z)\right] dw\,dz$$

Since the integration with respect to x and y is independent of the integration with respect to w and z, Eq. (II-7) may be rewritten as

$$I = \int_{-\infty}^{\infty}\int_{-\infty}^{\infty}\int_{-\infty}^{\infty}\int_{-\infty}^{\infty} A(x,y)A(w,z)\cos\left[\frac{\alpha x}{\lambda} + \frac{\beta y}{\lambda} + \phi(x,y)\right] \cdot$$
$$\cdot \cos\left[\frac{\alpha w}{\lambda} + \frac{\beta z}{\lambda} + \phi(w,z)\right] dx\,dy\,dw\,dz +$$
$$+ \int_{-\infty}^{\infty}\int_{-\infty}^{\infty}\int_{-\infty}^{\infty}\int_{-\infty}^{\infty} A(x,y)\,A(w,z)\sin\left[\frac{\alpha x}{\lambda} + \frac{\beta y}{\lambda} + \phi(x,y)\right] \cdot \qquad \text{(II-8)}$$
$$\cdot \sin\left[\frac{\alpha w}{\lambda} + \frac{\beta z}{\lambda} + \phi(w,z)\right] dx\,dy\,dw\,dz$$

By using the trigonometric identity

$$\cos a \cos b + \sin a \sin b = \cos(a-b) \qquad \text{(II-9)}$$

Eq. (II-8) can be rewritten as

$$I = \int_{-\infty}^{\infty}\int_{-\infty}^{\infty}\int_{-\infty}^{\infty}\int_{-\infty}^{\infty} A(x,y)\,A(w,z)\cos\left[\frac{\alpha x}{\lambda} + \frac{\beta y}{\lambda} + \right.$$
$$\left. + \phi(x,y) - \frac{\alpha w}{\lambda} - \frac{\beta z}{\lambda} - \phi(w,z)\right] dx\,dy\,dw\,dz \qquad \text{(II-10)}$$

Let

$$w = x + \epsilon_x, \quad dw = d\epsilon_x$$
$$z = y + \epsilon_y, \quad dz = d\epsilon_y$$

then

$$I = \int_{-\infty}^{\infty}\int_{-\infty}^{\infty}\int_{-\infty}^{\infty}\int_{-\infty}^{\infty} A(x,y)\,A(x+\epsilon_x, y+\epsilon_y)\cos\left[-\frac{\alpha\epsilon_x}{\lambda} - \frac{\beta\epsilon_y}{\lambda} + \right.$$
$$\left. + \phi(x,y) - \phi(x+\epsilon_x, y+\epsilon_y)\right] dx\,dy\,d\epsilon_x\,d\epsilon_y \qquad \text{(II-11)}$$

By using the trigonometric identity

$$\cos(a+b) = \cos a \cos b - \sin a \sin b \tag{II-12}$$

Eq. (II-11) becomes

$$I = \int_{-\infty}^{\infty}\int_{-\infty}^{\infty} \cos\left[\frac{\alpha\epsilon_x}{\lambda} + \frac{\beta\epsilon_y}{\lambda}\right]\left\{\int_{-\infty}^{\infty}\int_{-\infty}^{\infty} A(x,y)\,A(x+\epsilon_x, y+\epsilon_y)\cdot \right. \tag{II-13}$$

$$\left. \cdot \cos\left[\phi(x,y) - \phi(x+\epsilon_x, y+\epsilon_y)\right] dx\,dy\right\} d\epsilon_x\,d\epsilon_y +$$

$$+ \int_{-\infty}^{\infty}\int_{-\infty}^{\infty} \sin\left[\frac{\alpha\epsilon_x}{\lambda} + \frac{\beta\epsilon_y}{\lambda}\right]\left\{\int_{-\infty}^{\infty}\int_{-\infty}^{\infty} A(x,y)\,A(x+\epsilon_x, y+\epsilon_y)\cdot\right.$$

$$\left. \cdot \sin\left[\phi(x,y) - \phi(x+\epsilon_x, y+\epsilon_y)\right] dx\,dy\right\} d\epsilon_x\,d\epsilon_y$$

The terms

$$\left.\begin{aligned} G_1(\alpha,\beta) &= \cos\left[\frac{\alpha\epsilon_x}{\lambda} + \frac{\beta\epsilon_y}{\lambda}\right] \\ G_2(\alpha,\beta) &= \sin\left[\frac{\alpha\epsilon_x}{\lambda} + \frac{\beta\epsilon_y}{\lambda}\right] \end{aligned}\right\} \tag{II-14}$$

may be recognized as spatial frequency components where $\frac{\epsilon}{\lambda} = f$, and the double integral terms which multiply them in Eq. (II-13) is the transmittance associated with the spatial frequency (f_x, f_y). The transmittance of the cosine term is

$$T_c = \int_{-\infty}^{\infty}\int_{-\infty}^{\infty} A(x,y)\,A(x+\epsilon_x, y+\epsilon_y)\cdot$$

$$\cdot \cos\left[\phi(x,y) - \phi(x+\epsilon_x, y+\epsilon_y)\right] dx\,dy \tag{II-15}$$

and for the sine term

$$T_s = \int_{-\infty}^{\infty} \int_{-\infty}^{\infty} A(x,y)\, A(x+\epsilon_x, y+\epsilon_y) \cdot \cdot \sin\left[\phi(x,y) - \phi(x+\epsilon_x, y+\epsilon_y)\right] dx\, dy \qquad \text{(II-16)}$$

It must be remembered that A has nonzero value only over the region of the entrance pupil. The transmittance may be seen to be determined by pairs of points on the entrance pupil separated by a distance ϵ_x in the x direction, and ϵ_y in the y direction. It is further noted that it is the product of the amplitudes of the pairs of points and the difference in electromagnetic phase between the pairs of points which determine the transmittance.

This leads directly to the concept of Spatial Frequency Zones on the entrance pupil. For a given spatial frequency (f_x, f_y), those regions of the entrance pupil which contribute to the generation of this spatial frequency are defined by bounding all pairs of points which are separated by a distance ϵ_x in the x direction and ϵ_y in the y direction.

Equations (II-15) and (II-16) are the transmittance values which result from both the atmospheric turbulence and the diffraction limit of the optical system. To make this point clear, the transmittance in the absence of the phase disturbance will be derived. When $\Delta\phi = 0$

$$T_{cd} = \int_{-\infty}^{\infty} \int_{-\infty}^{\infty} A_o(x,y)\, A_o(x+\epsilon_x, y+\epsilon_y)\, dx\, dy \qquad \text{(II-17)}$$

and

$$T_{sd} = 0 \qquad \text{(II-18)}$$

If A_o is constant over the entrance pupil, then Eq. (II-17) is

$$T_{cd} = A_o^2 S_\epsilon \tag{II-19}$$

where S_ϵ is the area of the spatial frequency zone associated with the spatial frequency (f_x, f_y). Equation (II-19) is a useful tool in determining the transfer function for a diffraction limited optical system.

The transfer function which may be attributed to the turbulence alone is found by dividing (II-16) by (II-19). Expressed in complex form the transfer function for the turbulence is

$$t = \frac{T_c + j T_s}{A_o^2 S_\epsilon} \tag{II-20}$$

The concept of spatial frequency zones makes it clear that there is a sharp cutoff to the spatial frequencies transmitted by an optical system. Since the largest separation possible for a pair of points is equal to the maximum dimension of the entrance pupil, D, the highest spatial frequency passed by the optical system is

$$f_{max} = \frac{D}{\lambda} \tag{II-21}$$

This is the Fourier equivalent of the usual diffraction limit expression that the angular distance to the first null of the diffraction pattern is

$$\alpha = \frac{1.22\,\lambda}{D} \tag{II-22}$$

Appendix III.

Development of restoration factors for temporally invariant distortion.

Section A treats the one-dimensional case and section B treats the two-dimensional case.

Section A.

Development of restoration factors for one-dimensional temporally invariant distortion.

Immediately following this page is a graphical representation of the distortion process. The number of divisions was arbitrarily chosen to show the difference in the effect of odd and even numbers of divisions.

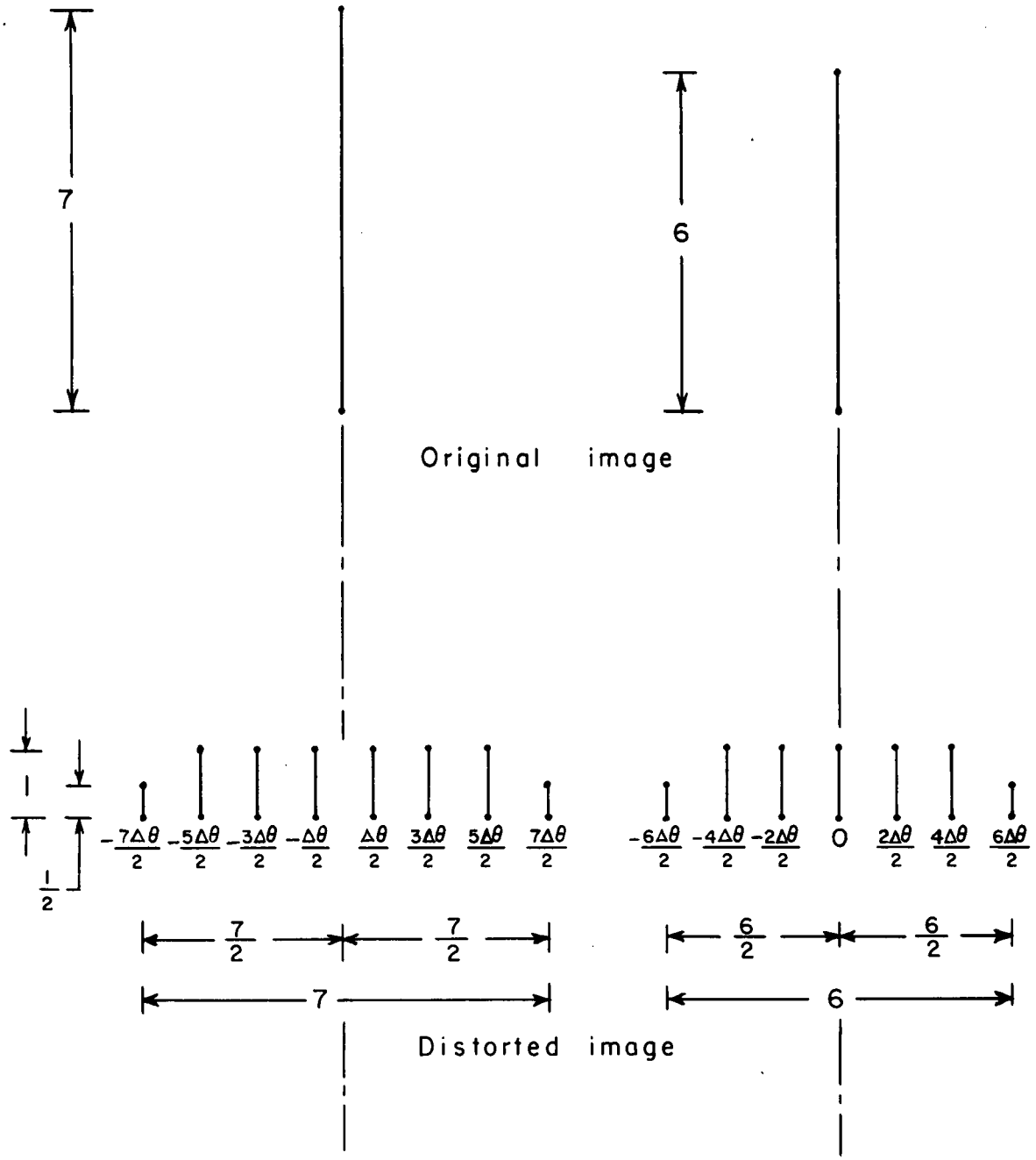

Graphical representation of distortion process

Notation:

$F(\theta)$: Fourier representation of original image.

$f(\theta)$: Fourier representation of distorted image.

$g(\theta)$: Fourier representation of an element of distorted image.

F_k: k-th term of $F(\theta)$

f_k: k-th term of $f(\theta)$

g_k: k-th term of $g(\theta)$

θ: range of region considered. $0 \leq \theta \leq 2\pi$.

$\Delta\theta$: Angular separation of elements of distorted image.

$r\Delta\theta$: Angular distance of a distortion element from center of distortion. $r = \frac{s}{2} - i \geq 0$, $i = 0, 1, \cdots$.

s: Number of divisions of distortion (number of elements less 1).

a, b : Fourier coefficients of f, indexed by k,

$$0 \le k \le \frac{m-1}{2} = n$$

A, B : Fourier coefficients of F, indexed by k,

$$0 \le k \le \frac{m-1}{2} = n$$

m : Number of input points of entire image.

n : highest index of coefficients, $n = \frac{m-1}{2}$.

p: $p = \frac{1}{s}$, $r \neq \frac{s}{2}$

$= \frac{1}{2s}$, $r = \frac{s}{2}$

q: $q = 2p$, $r \neq 0$ or $q = \frac{2}{s}$, $r \neq \frac{s}{2}$, 0

$= p$, $r = 0$ $= \frac{1}{s}$, $r = \frac{s}{2}$, 0

$$F(\theta) = \sum_{k=0}^{n} (A_k \cos k\theta + B_k \sin k\theta) \qquad (1)$$

Let: $F_k(\theta) = A_k \cos k\theta + B_k \sin k\theta$

Then: $F(\theta) = \sum_k F_k(\theta) \qquad (2)$

$$f(\theta) = \sum_{r=-\frac{S}{2}}^{\frac{S}{2}} g(\theta + r\Delta\theta)$$

where: $g(\theta + r\Delta\theta) = \sum_k p[A_k \cos k(\theta + r\Delta\theta) + B_k \sin k(\theta + r\Delta\theta)$

Let: $g_k(\theta + r\Delta\theta) = p[A_k \cos k(\theta + r\Delta\theta) + B_k \sin k(\theta + r\Delta\theta)$

$$f(\theta) = \sum_r \sum_k g_k(\theta + r\Delta\theta)$$

Assuming convergence of the series g (Fourier series, Hardy, MacMillan, 1944, p. 37 ff.; Theory of Fourier Series and Integrals, Carslaw, Dover, Third edition, 1930, p. 230 ff.).

$$f(\theta) = \Sigma_k \Sigma_r g_k(\theta + r\Delta\theta)$$

Let: $f_k = \Sigma_r g_k(\theta + r\Delta\theta)$ (3)

$$f(\theta) = \Sigma_k f_k \quad (4)$$

Expanding: $g_k(\theta + r\Delta\theta) =$

$$= p[A_k(\cos k\theta \cos kr\Delta\theta - \sin k\theta \sin kr\Delta\theta) +$$

$$+ B_k(\sin k\theta \cos kr\Delta\theta + \cos k\theta \sin kr\Delta\theta)$$

In summing $g_k(\theta + r\Delta\theta)$ over $r = -\frac{s}{2}, \frac{s}{2}$, since $\sin x = -\sin(-x)$ and $\sin 0 = 0$, the terms containing $\sin kr\Delta\theta$ will vanish.

$$\Sigma_r g_k(\theta + r\Delta\theta) = \Sigma_r p \cos kr\Delta\theta (A_k \cos k\theta +$$

$$+ B_k \sin k\theta)$$

Or from (3): $f_k = F_k \Sigma_r p \cos kr\Delta\theta$

Substituting in (4): $f(\theta) = \Sigma_k F_k \Sigma_r p \cos kr\Delta\theta$

It is now evident that f_k is the k-th term of the Fourier series representing $f(\theta)$. So from (1) and the independence or orthogonality of the sin and cos terms:

$$a_k = A_k \Sigma_r p \cos kr\Delta\theta$$

$$b_k = B_k \Sigma_r p \cos kr\Delta\theta$$

Then:

$$A_k = \frac{a_k}{\Sigma_r p \cos kr\Delta\theta}$$

$$B_k = \frac{b_k}{\Sigma_r p \cos kr\Delta\theta}$$

The last expressions can be simplified for computation by folding the summation, since $\cos(x) = \cos(-x)$. The

problem of odd and even numbers of intervals is taken care of by the condition $r \geq 0$ and by the substitution of q for p. (See notation list).

$$A_k = \frac{a_k}{\sum_{i=0}^{\frac{S}{2}} q \cos kr\,\Delta\theta}$$

$$B_k = \frac{b_k}{\sum_{i=0}^{\frac{S}{2}} q \cos kr\,\Delta\theta}$$

Section B.

Development of restoration factors for two-dimensional temporally invariant distortion.

Immediately following this sheet are graphical representations of the temporally invariant distortion process. In these representations each square represents a point value of the image brightness. The number of divisions was arbitrarily chosen to show the difference in effect of odd and even numbers of divisions.

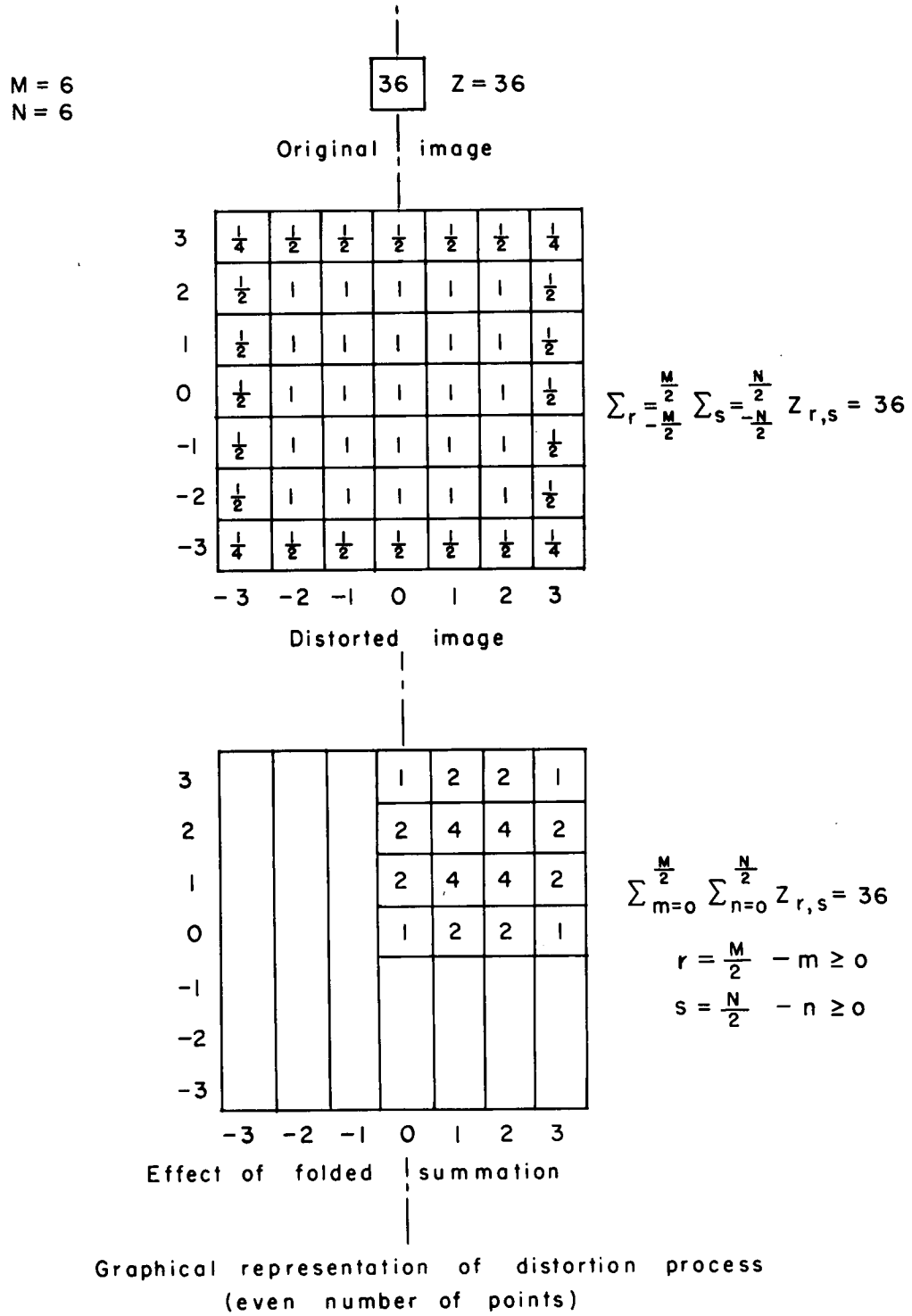

Graphical representation of distortion process
(even number of points)

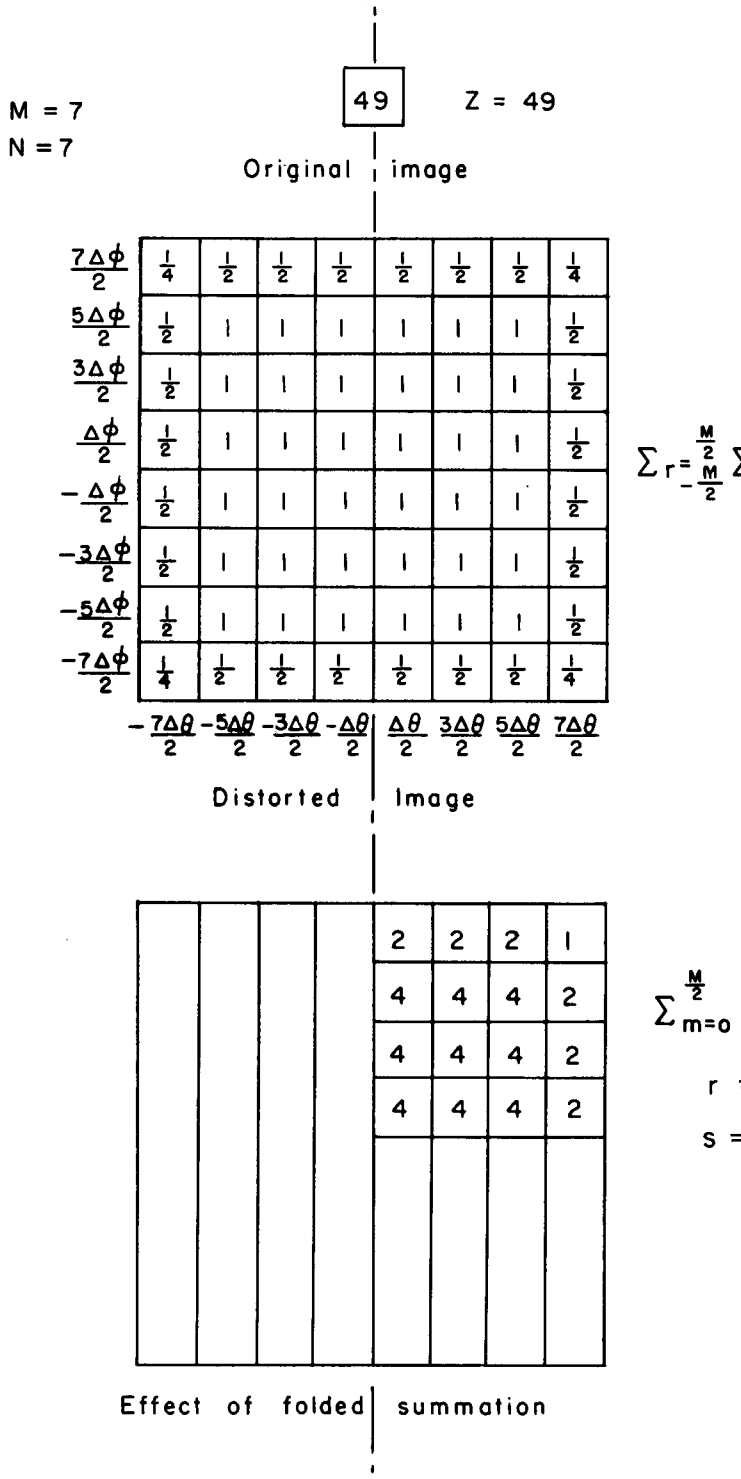

Graphical representation of distortion process
(odd number of points)

Notation:

C, D, E, F: Fourier coefficients with respect to $\Xi(\theta, \Phi)$

c, d, e, f: Fourier coefficients with respect to $\xi(\theta, \Phi)$

ζ: an element of the distorted image.

I: limit on x of number of terms of Fourier series.

J: limit on y of number of terms of Fourier series.

i: index on x of terms, $i = 0, 1, \cdots, I$

j: index on y of terms, $j = 0, 1, \cdots, J$

M: number of divisions of distortion on x. Points are $M+1$

N: number of divisions of distortion on y. Points are $N+1$

m: index on x of points of distortion, $m = -\frac{M}{2}, \frac{M}{2}$

n: index on y of points of distortion, $n = -\frac{N}{2}, \frac{N}{2}$

p: weighting factor; $p = 1, r \neq \pm \frac{M}{2}, s \neq \pm \frac{N}{2}$

$= \frac{1}{2}, r = \pm \frac{M}{2}, s \neq \pm \frac{N}{2}$

$= \frac{1}{2}, r \neq \pm \frac{M}{2}, s = \pm \frac{N}{2}$

$= \frac{1}{4}, r = \pm \frac{M}{2}, s = \pm \frac{N}{2}$

q: weighting factor: $q = 4; r \neq 0, \frac{M}{2}; s \neq 0, \frac{N}{2}$

$= 2; r = 0, \frac{M}{2}; s \neq 0, \frac{N}{2}$

$= 2; r \neq 0, \frac{M}{2}; s = 0, \frac{N}{2}$

$= 1; r = 0, \frac{M}{2}; s = 0, \frac{N}{2}$

r: multiplier of $\Delta\theta$: $r\Delta\theta$ is angular distance on x of element from center of distortion. $r = \frac{M}{2} - m \geq 0$

s: multiplier of $\Delta\phi$: $s\Delta\phi$ is angular distance ony of element from center of distortion. $s = \frac{N}{2} - n \geq 0$

x : abscissa of image field.

y : ordinate of image field.

$Z(\theta,\phi)$: Fourier representation of undistorted image.

$z(\theta,\phi)$: Fourier representation of distorted image.

θ : angular measure on x of field

ϕ : angular measure on y of field

Given:

$$Z(\theta,\phi) = \sum_{i=0}^{I} \sum_{j=0}^{J} \left(C_{ij} \cos i\theta \cos j\phi + D_{ij} \cos i\theta \sin j\phi + \right.$$

$$\left. + E_{ij} \sin i\theta \cos j\phi + F_{ij} \sin i\theta \sin j\phi \right)$$

Let: $Z_{ij}(\theta,\phi) = C_{ij} \cos i\theta \cos j\phi + D_{ij} \cos i\theta \sin j\phi +$

$$+ E_{ij} \sin i\theta \cos j\phi + F_{ij} \sin i\theta \sin j\phi \quad (1)$$

$$Z(\theta,\phi) = \sum_i \sum_j Z_{ij}(\theta,\phi)$$

$$z(\theta,\phi) = \sum_{r=-\frac{M}{2}}^{\frac{M}{2}} \sum_{s=-\frac{N}{2}}^{\frac{N}{2}} g(\theta + r\Delta\theta, \phi + s\Delta\phi)$$

Where: $g(\theta + r\Delta\theta, \phi + s\Delta\phi) =$

$$= \sum_i \sum_j p[C_{ij} \cos i(\theta + r\Delta\theta) \cos j(\phi + s\Delta\phi) +$$

$$+ D_{ij} \cos i(\theta + r\Delta\theta) \sin j(\phi + s\Delta\phi) +$$

$$+ E_{ij} \sin i(\theta + r\Delta\theta) \cos j(\phi + s\Delta\phi) +$$

$$+ F_{ij} \sin i(\theta + r\Delta\theta) \sin j(\phi + s\Delta\phi)$$

Let $g_{ij}(\theta + r\Delta\theta, \phi + s\Delta\phi) = p[C_{ij} \cos i(\theta + r\Delta\theta) \cos j(\phi + s\Delta\phi) +$

$$+ D_{ij} \cos i(\theta + r\Delta\theta) \sin j(\phi + s\Delta\phi) +$$

$$+ E_{ij} \sin i(\theta + r\Delta\theta) \cos j(\phi + s\Delta\phi) +$$

$$+ F_{ij} \sin i(\theta + r\Delta\theta) \sin j(\phi + s\Delta\phi) \quad (2)$$

$$z = \sum_r \sum_s \sum_i \sum_j g_{ij}(\theta + r\Delta\theta, \phi + s\Delta\phi)$$

Assuming convergence of series as in Section A:

$$z = \Sigma_i \Sigma_j \left(\Sigma_r \Sigma_s \zeta_{ij} \right)$$

Let: $$z_{ij} = \Sigma_r \Sigma_s \zeta_{ij} \qquad (3)$$

Then: $$z = \Sigma_i \Sigma_j z_{ij} \qquad (4)$$

Expanding (2): $\zeta_{ij}(\theta + r\Delta\theta, \phi + s\Delta\phi) =$

$$= p[C_{ij}(\cos i\theta \cos ir\Delta\theta - \sin i\theta \sin ir\Delta\theta) \cdot$$

$$\cdot (\cos j\phi \cos js\Delta\phi - \sin j\phi \sin js\Delta\phi) +$$

$$+ D_{ij}(\cos i\theta \cos ir\Delta\theta - \sin i\theta \sin ir\Delta\theta) \cdot$$

$$\cdot (\sin j\phi \cos js\Delta\phi + \cos j\phi \sin js\Delta\phi) +$$

$$+ E_{ij}(\sin i\theta \cos ir\Delta\theta + \cos i\theta \sin ir\Delta\theta) \cdot$$

$$\cdot (\cos j\phi \cos js\Delta\phi - \sin j\phi \sin js\Delta\phi) +$$

$$+ F_{ij} (\sin i\theta \cos ir\Delta\theta + \cos i\theta \sin ir\Delta\theta) \cdot$$

$$\cdot (\sin j\phi \cos js\Delta\phi + \cos j\phi \sin js\Delta\phi)$$

In summing ζ_{ij}, above, over $r = -\frac{M}{2}, \frac{M}{2}$, and $s = -\frac{N}{2}, \frac{N}{2}$, terms containing $\sin ir\Delta\theta$ and $\sin js\Delta\phi$ will vanish since $\sin x = -\sin(-x)$ and $\sin 0 = 0$.

$$\Sigma_r \Sigma_s \zeta_{ij}(\theta + r\Delta\theta, \phi + s\Delta\phi) = \Sigma_r \Sigma_s p \cos ir\Delta\theta \cos js\Delta\phi \cdot$$

$$\cdot [C_{ij} \cos i\theta \cos j\phi + D_{ij} \cos i\theta \sin j\phi +$$

$$+ E_{ij} \sin i\theta \cos j\phi + F_{ij} \sin i\theta \sin j\phi]$$

From (3) and (1): $z_{ij} = Z_{ij} \Sigma_r \Sigma_s p \cos ir\Delta\theta \cos js\Delta\phi$, and substituting in (4):

$$Z(\theta,\phi) = \Sigma_i \Sigma_j Z_{ij} \Sigma_r \Sigma_s p \cos ir\Delta\theta \cos js\Delta\phi$$

It is now evident that Z_{ij} is the (i,j)th term of the Fourier series representing $Z(\theta,\phi)$. From the independence or orthogonality of the component terms:

$$Z_{ij} = \frac{Z_{ij}}{\sum_r \sum_s p \cos ir\Delta\theta \cos js\Delta\phi}$$

$$C_{ij} = \frac{C_{ij}}{\sum_r \sum_s p \cos ir\Delta\theta \cos js\Delta\phi}$$

and likewise for D, E, and F with respect to d, e and f of z_{ij}.

As in Section A, the denominator above can be simplified for computation by folding the summations, since $\cos x = \cos(-x)$. The problem of odd and even intervals is taken care of by the conditions $r \geq 0, s \geq 0$ and by

the substitution of q for p. The denominator then becomes:

$$\sum_{m=0}^{\frac{M}{2}} \sum_{n=0}^{\frac{N}{2}} q \cos ir\Delta\theta \cos js\Delta\phi$$

where $r = \frac{M}{2} - m \geq 0$

$$s = \frac{N}{2} - n \geq 0$$

William Hadley Richardson

Appendix IV.

Restoration of images with Temporally variant distortion.

Section A treats the one-dimensional case and section B treats the two-dimensional case.

Section A.

Restoration of one-dimensional image with Temporally variant distortion.

Given: A number of distorted images indexed $j = 1, 2, \cdots$, each represented by a Fourier series with coefficients $A_{i,j}$ and $B_{i,j}$ indexed with respect to frequency by $i = 1, 2, \cdots$.

To find: The restored coefficients, A_a and B_a

Conditions:

(1) $A_a^2 + B_a^2 = \max_j \left(A_{a,j}^2 + B_{a,j}^2 \right)$

$$(2)\quad \frac{A_a}{B_a} = \frac{\sum_j A_{a,j}}{\sum_j B_{a,j}}$$

$$(3)\quad sgn(A_a) = sgn\left(\sum_j A_{a,j}\right)$$

$$(4)\quad sgn(B_a) = sgn\left(\sum_j B_{a,j}\right)$$

Solution:

$$A_a = B_a \frac{\sum_j A_{a,j}}{\sum_j B_{a,j}} \quad ; \text{ from (2)}$$

Substituting in (1):

$$\left(B_a \frac{\sum_j A_{a,j}}{\sum_j B_{a,j}}\right)^2 + B_a^2 = \max_j\left(A_{a,j}^2 + B_{a,j}^2\right)$$

$$B_a\left(\frac{\sum_j^2 A_{a,j}}{\sum_j^2 B_{a,j}} + 1\right) = \max_j\left(A_{a,j}^2 + B_{a,j}^2\right)$$

$$B_a = \left|\left[\frac{\max_j\left(A_{a,j}^2 + B_{a,j}^2\right)}{\frac{\sum_j^2 A_{a,j}}{\sum_j^2 B_{a,j}} + 1}\right]^{1/2}\right| \cdot sgn\left(\sum_j B_{a,j}\right)$$

$$A_a = \left|B_a \frac{\sum_j A_{a,j}}{\sum_j B_{a,j}}\right| \cdot sgn\left(\sum_j A_{a,j}\right)$$

Section B.

Restoration of Two-dimensional image with Temporally variant distortion.

Given: A number of distorted images indexed $m = 1, 2, \cdots$, each represented by a Fourier series:

$$f_m(\theta_k, \phi_l) = \sum_i \sum_j \left(C_{ijm} \cos i\theta_k \cos j\phi_l + \right.$$

$$+ D_{ijm} \cos i\theta_k \sin j\phi_l + E_{ijm} \sin i\theta_k \cos j\phi_l +$$

$$\left. + F_{ijm} \sin i\theta_k \sin j\phi_l \right)$$

The given equation can be rewritten as:

$$f_m(\theta_k, \phi_l) = \frac{1}{2} \sum_i \sum_j \left[(C_{ijm} - F_{ijm}) \cos(i\theta_k + j\phi_l) + \right.$$

$$+ (C_{ijm} + F_{ijm}) \cos(i\theta_k - j\phi_l) +$$

$$+ (D_{ijm} + E_{ijm}) \sin(i\theta_k + j\phi_l) +$$

$$\left. + (-D_{ijm} + E_{ijm}) \sin(i\theta_k - j\phi_l) \right]$$

Since the restoration process is the same for each (i,j), the i and j notation is dropped in the following.

To find: The restored coefficients C', D, E, F.

Conditions:

(100) $$(C-F)^2+(D+E)^2 = \max_m\left[(C_m-F_m)^2+(D_m+E_m)^2\right] = (\#1)$$

(101) $$(C+F)^2+(-D+E)^2 = \max_m\left[(C_m+F_m)^2+(-D_m+E_m)^2\right] = (\#2)$$

(102) $$\frac{C-F}{D+E} = \frac{\sum_m (C_m-F_m)}{\sum_m (D_m+E_m)} = (\#3)$$

(103) $$\frac{C+F}{-D+E} = \frac{\sum_m (C_m+F_m)}{\sum_m (-D_m+F_m)} = (\#4)$$

(104) $$\operatorname{sgn}(C-F) = \operatorname{sgn}\left[\sum_m (C_m-F_m)\right]$$

(105) $$\operatorname{sgn}(C+F) = \operatorname{sgn}\left[\sum_m (C_m+F_m)\right]$$

(106) $$\operatorname{sgn}(D+E) = \operatorname{sgn}\left[\sum_m (D_m+E_m)\right]$$

(107) $$\operatorname{sgn}(-D+E) = \operatorname{sgn}\left[\sum_m (-D_m+E_m)\right]$$

(102.1) From (102): $(C-F)^2 = (D+E)^2 \cdot (\#3)^2$

(103.1) From (103): $(C+F)^2 = (-D+E)^2 \cdot (\#4)^2$

Substituting (102.1) in (100) and (103.1) in (101):

(108) $(D+E)^2 \cdot (\#3)^2 + (D+E)^2 = (\#1)$

(109) $(-D+E)^2 \cdot (\#4)^2 + (-D+E)^2 = (\#2)$

From (108) and (106):

(110) $$(D+E) = \left| \left[\frac{(\#1)}{(\#3)^2+1} \right]^{1/2} \right| \cdot \operatorname{sgn}\left[\Sigma_m (D_m + E_m)\right] = (\#6)$$

From (109) and (107):

(111) $$(-D+E) = \left| \left[\frac{(\#1)}{(\#4)^2+1} \right]^{1/2} \right| \cdot \operatorname{sgn}\left[\Sigma_m (-D_m + E_m)\right] = (\#8)$$

(102.2) From (102): $(D+E)^2 = \frac{1}{(\#3)^2}(C-F)^2$

(103.2) From (103): $(-D+E)^2 = \frac{1}{(\#4)^2}(C+F)^2$

Substituting (102.2) in (100):

$$(112)\quad (C-F)^2 + \frac{1}{(\#3)^2}(C-F)^2 = (\#1)$$

Substituting (103.2) in (101):

$$(113)\quad (C+F)^2 + \frac{1}{(\#4)}(C+F)^2 = (\#2)$$

From (112) and (104):

$$(114)\quad (C-F) = \left|\left[\frac{(\#1)}{\frac{1}{(\#3)^2}+1}\right]^{1/2}\right| \cdot \operatorname{sgn}\left[\Sigma_m (C_m - F_m)\right] = (\#5)$$

From (113) and (105):

$$(115)\quad (C+F) = \left|\left[\frac{(\#2)}{\frac{1}{(\#4)^2}+1}\right]^{1/2}\right| \cdot \operatorname{sgn}\left[\Sigma_m (C_m + F_m)\right] = (\#7)$$

Adding (114) and (115):

$$C = \frac{(\#5) + (\#7)}{2}$$

$$\text{Or: } C = \frac{1}{2}\left|\left\{\frac{\max_m\left[(C_m - F_m)^2 + (D_m + E_m)^2\right]}{\left[\frac{\Sigma_m(D_m+E_m)}{\Sigma_m(C_m-F_m)}\right]^2 + 1}\right\}^{1/2}\right| \cdot \operatorname{sgn}\left[\Sigma_m(C_m-F_m)\right] +$$

$$+\frac{1}{2}\left|\left\{\frac{\max_m\left[(C_m+F_m)^2 + (-D_m+E_m)^2\right]}{\left[\frac{\Sigma_m(-D_m+E_m)}{\Sigma_m(C_m+F_m)}\right]^2 + 1}\right\}^{1/2}\right| \cdot \operatorname{sgn}\left[\Sigma_m(C_m+F_m)\right]$$

Subtracting (111) from (110):

$$D = \frac{(\#6) - (\#8)}{2}$$

$$\text{Or: } D = \frac{1}{2}\left|\left\{\frac{\max_m\left[(C_m - F_m)^2 + (D_m + E_m)^2\right]}{\left[\frac{\Sigma_m(C_m-F_m)}{\Sigma_m(D_m+E_m)}\right]^2 + 1}\right\}^{1/2}\right| \cdot \operatorname{sgn}\left[\Sigma_m(D_m+E_m)\right] -$$

$$-\frac{1}{2}\left|\left\{\frac{\max_m\left[(C_m+F_m)^2 + (-D_m+E_m)^2\right]}{\left[\frac{\Sigma_m(C_m+F_m)}{\Sigma_m(-D_m+E_m)}\right]^2 + 1}\right\}^{1/2}\right| \cdot \operatorname{sgn}\left[\Sigma_m(-D_m+F_m)\right]$$

Adding (110) and (111):

$$E = \frac{(\#6) + (\#8)}{2}$$

$$\text{Or } E = \frac{1}{2}\left|\left\{\frac{\max_m\left[(C_m - F_m)^2 + (D_m + E_m)^2\right]}{\left[\frac{\Sigma_m(C_m - F_m)}{\Sigma_m(D_m + E_m)}\right]^2 + 1}\right\}^{1/2}\right| \cdot \operatorname{sgn}\left[\Sigma_m(D_m + E_m)\right] +$$

$$+ \frac{1}{2}\left|\left\{\frac{\max_m\left[(C_m + F_m)^2 + (-D_m + E_m)^2\right]}{\left[\frac{\Sigma_m(C_m + F_m)}{\Sigma_m(-D_m + E_m)}\right]^2 + 1}\right\}^{1/2}\right| \cdot \operatorname{sgn}\left[\Sigma_m(-D_m + E_m)\right]$$

Subtracting (114) from (115):

$$F = \frac{-(\#5) + (\#7)}{2}$$

$$\text{Or } F = -\frac{1}{2}\left|\left\{\frac{\max_m\left[(C_m - F_m)^2 + (D_m + E_m)^2\right]}{\left[\frac{\Sigma_m (D_m + F_m)}{\Sigma_m (C_m - F_m)}\right]^2 + 1}\right\}^{1/2}\right| \cdot \operatorname{sgn}\left[\Sigma_m (C_m - F_m)\right] +$$

$$+\frac{1}{2}\left|\left\{\frac{\max_m\left[(C_m + F_m)^2 + (-D_m + E_m)^2\right]}{\left[\frac{\Sigma_m (-D_m + E_m)}{\Sigma_m (C_m + F_m)}\right]^2 + 1}\right\}^{1/2}\right| \cdot \operatorname{sgn}\left[\Sigma_m (C_m + F_m)\right]$$

William Hadley Richardson

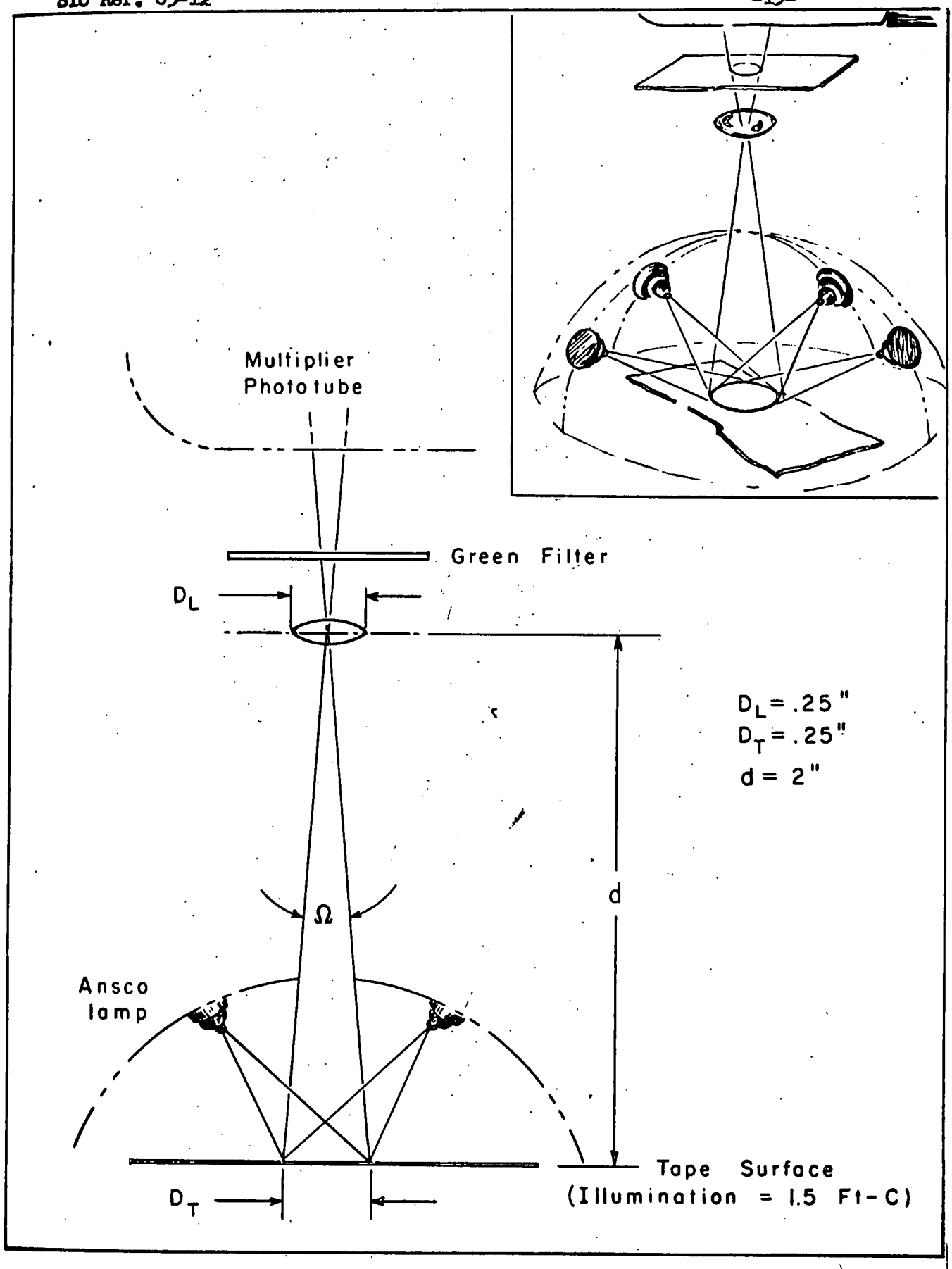

Figure 6 - Schematic representation of the Ansco reflection head.

calculated as follows:

$$F = B \Omega A \qquad \text{where } B = Ir, \quad \Omega = \frac{A_t}{d^2}$$

B = surface brightness in foot-lamberts

r = surface reflectance

I = surface illumination in foot candles

Ω = solid angle in steradians

A_L = lens area in ft^2

The illumination on the tape surface was measured at 1.5 (ft-candles). Using this value of illumination and taking a unity surface reflectance, one has,

$$B = 1.5 \text{ (ft-candles)} \times 1\text{(ft-lamberts/ft-candles)} = 1.5\text{(ft-lamberts)}$$

$$\Omega = \frac{\pi D_t^2}{4} \times \frac{1}{d^2} = \frac{\pi}{4} \times \frac{1}{.25^2} \times \frac{1}{2^2} = 1.25 \times 10^{-2} \text{ steradians}$$

$$A_L = \frac{\pi D_L^2}{4} = \frac{\pi \times .25^2}{4} \times \frac{1}{144} = 3.4 \times 10^{-4} \text{ ft}^2$$

$$F = 1.25 \times 10^{-2} \text{ (steradians)} \times 3.4 \times 10^{-4} \text{ (ft}^2\text{)} \times 1.5 \text{ (ft-lamberts)}$$
$$= 6.38 \times 10^{-6} \text{ lumens}$$

The cathode current for this value of flux would be,

$$i_c = s_2 F$$

For a 931-A a typical value of s_2 is 30 (microamps/lumen).

$$i_o = 30 \text{ (microamps/lumen)} \times 6.38 \times 10^{-6} \text{ (lumens)}$$
$$= 1.914 \times 10^{-4} \text{ (microamps)}$$

The fractional reduction in current that would result when the flux is filtered by the green Ansco filter would be found as before by the ratio,

$$\frac{S_2'}{S_2} = w \frac{\int_0^\infty J(\lambda)\ S_2(\lambda)\ W(\lambda)\ d\lambda}{\int_0^\infty J(\lambda)\ S_2(\lambda)\ d\lambda}$$

$$= w \frac{.524}{6.45} = .0812\ w$$

where $J(\lambda)$ is the spectral emittance of a 2854° K full radiator

$S_2(\lambda)$ is the normalized photomultiplier tube response

$W(\lambda)$ is the normalized response of the green Ansco filter

w is the peak transmittance of the green Ansco filter

Figure 7 illustrates this process.

Taking a value of unity for w, the photocathode current resulting from the filtered flux is,

$$i_o' = 1.914 \times 10^{-4} \text{(microamps)} \times .0812 = 1.55 \times 10^{-5} \text{ (microamps)}$$

Now it is quite possible to achieve a stable gain in the order of 10^6 from a multiplier phototube, depending upon the value of dynode voltage employed. In the case of the circuit actually used the value of dynode voltage used was 1,200 volts resulting in a median gain of 2×10^6.

$$i_a' = 1.55 \times 10^{-5} \text{ (microamps)} \times 2 \times 10^6 = 31 \text{ (microamps)}$$

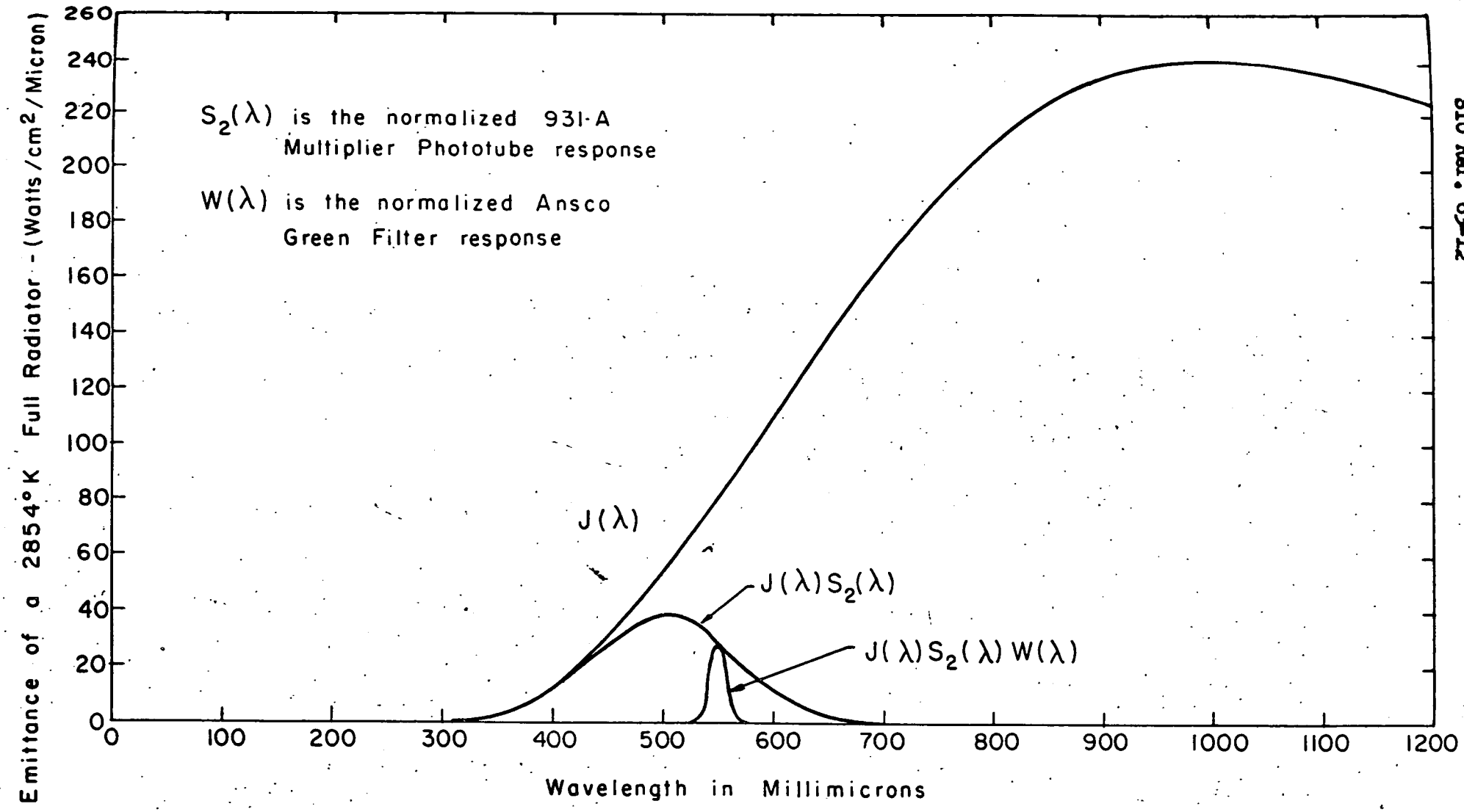

Figure 7 - Spectral curves showing the relative amounts of radiator power utilized by the Multiplier Phototube before and after filtering.

In practice this current could be set at 40 (microamps) for the yellow tape by a slight adjustment of the lamp supply voltage. The red tape then yielded a 20 (microamp) signal as would be predicted by comparing the spectral reflectance curves of the two tapes in the green part of the spectrum.

When a multiplier phototube is used as a detector, no additional filtering is needed to eliminate the near infra-red radiation since the S-4 surface is not responsive in this region. Hence, in spite of the low signal current at the photocathode the 931-A multiplier phototube proved to be a superior detector for this application.

5. CIRCUIT DESIGN DETAILS

The electronic system can be naturally subdivided into three sections, the high voltage supply, the lamp supply, and the amplifier. The high voltage supply is the most critical component of the system as far as stability is concerned, since the multiplier phototube gain varies as the nth power of the dynode voltage, n being an exponent that varies from tube to tube but typically has a value on the order of 5 or 6. The high voltage supply used in this system was a 2,000 volt, 2 milliamp supply manufactured by the Condenser Products Company. This supply was used since it was already at hand. Additional stability was added by driving the supply with a Sola constant voltage transformer (not shown on the schematic) and regulating the output with a Victoreen Corona discharge regulator. A more logical supply to use for this application would be a solid state dc to dc convertor type. A

regulated supply of this type is manufactured and it would be much more compact.

Second in importance to the high voltage supply is the lamp supply. Here the flux varies as approximately the 3.5 power of the voltage, so this supply also must be regulated if the device is to be made insensitive to line voltage changes. A compound regulation effect is simply achieved by employing a Sola constant voltage transformer as the rectifier transformer and following the output of the power supply with a compound connected emitter follower. The lamps are connected to the emitter and the base is held at a constant voltage by means of a zener diode.

The amplifier must perform two functions. First of all a power gain must be achieved to drive the 60millivolt relay with the .4 millivolts of available power at the photomultiplier anode. Secondly, a discrimination must be made between the 20 microamps of current produced by the red tape and the 40 microamps of current produced by the green tape.

The first 2N1375 transistor is an emitter follower which reflects the voltage change that occurs in the base circuit to the emitter but reduces the impedance level by a factor of the beta of the transistor (minimum value -50). The 1N755 zener diode is the discrimination element. The breakdown voltage of this diode occurs at 7.5 volts which is midway between the 5 volts resulting from the red tape and the 10 volts from the yellow tape. Once the diode breaks down, sufficient current is transferred to the base circuit of the second transistor to activate the relay in the collector circuit.

The circuit is fail safe since the function of the relay would be to turn on the unclassified tape reader. Any circuit or power failure would simply prevent the reader from turning on when tape was fed into the machine.

The device was found to be quite reliable and stable in operation. Also there is a good insensitivity to line voltage variation. The line voltage can be varied from 70 to 140 volts and the anode current will hold constant over this range dropping 5 per cent at each end. Long term drift does not appear to be a problem. After a short warm up period the anode current holds constant throughout the day.

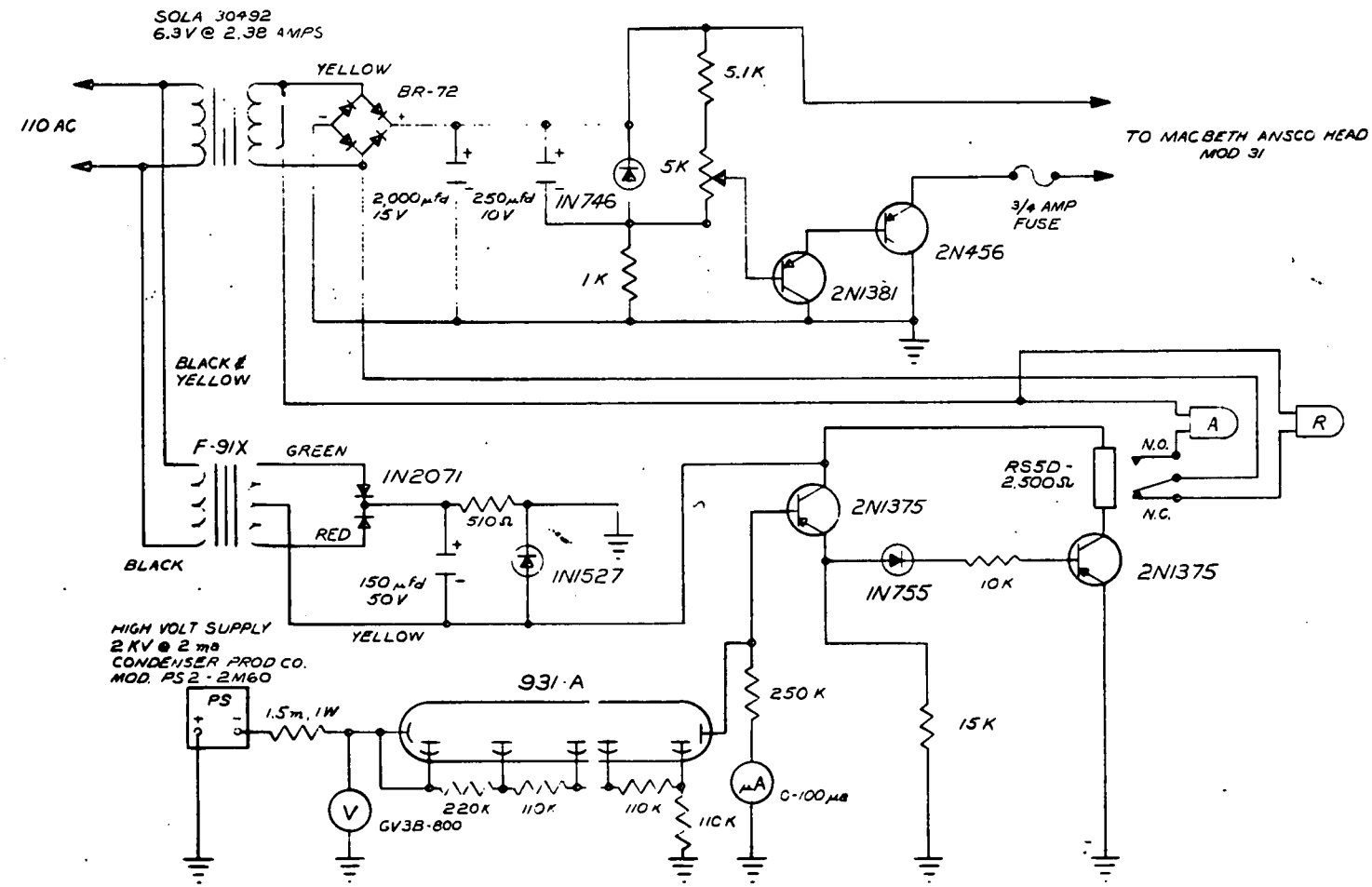

ELECTRICAL SCHEMATIC OF THE COLORED TELETYPE TAPE DISCRIMINATION